Combustion and Flame 233 (2021) 111557

Contents lists available at ScienceDirect

Combustion and Flame

journal homepage: www.elsevier.com/locate/combustflame

# Exploring the interaction kinetics of butene isomers and $NO_x$ at low temperatures and diluted conditions

Sabrina Gossler[a,1], Lena Ruwe[b,c,1], Wenhao Yuan[d,1], Jiuzhong Yang[e], Xiamin Chen[d], Steffen Schmitt[c], Lubow Maier[f], Katharina Kohse-Höinghaus[c,*], Fei Qi[d,*], Olaf Deutschmann[a,f,*]

[a] Institute for Chemical Technology and Polymer Chemistry, Karlsruhe Institute of Technology (KIT), Engesserstraße 20, 76131 Karlsruhe, Germany
[b] Physikalisch-Technische Bundesanstalt (PTB), Bundesallee 100, 38116 Braunschweig, Germany
[c] Department of Chemistry, Bielefeld University, Universitätsstraße 25, 33615 Bielefeld, Germany
[d] Key Laboratory for Power Machinery and Engineering of MOE, Shanghai Jiao Tong University, Shanghai 200240, PR China
[e] National Synchrotron Radiation Laboratory, University of Science and Technology of China, Hefei, Anhui 230029, PR China
[f] Institute for Catalysis Research and Technology (IKFT), Karlsruhe Institute of Technology (KIT), Hermann-von-Helmholtz-Platz 1, 76344 Eggenstein-Leopoldshafen, Germany

ARTICLE INFO

*Article history:*
Received 13 February 2021
Revised 8 June 2021
Accepted 8 June 2021

*Keywords:*
Oxidation of butene isomers
NO butene interaction
Chemical kinetics
Low-temperature chemistry
SVUV-PIMS
Flow reactor
Combustion exhaust gases

ABSTRACT

The oxidation of 1-butene and *i*-butene with and without addition of 1000 ppm NO was experimentally and numerically studied primarily at fuel-rich ($\phi = 2.0$) conditions under high dilution (96% Ar) in a flow reactor operated at atmospheric pressure in the low temperature range of approximately 600-1200 K. Numerous intermediate species were detected and quantified using synchrotron vacuum ultraviolet photoionization mass spectrometry (SVUV-PIMS). An elementary-step reaction mechanism consisting of 3996 reactions among 682 species, based on literature and this work, was established to describe the reactions and interaction kinetics of the butene isomers with oxygen and nitrogenous components. Model predictions were compared with the experimental results to gain insight into the low- and high-temperature fuel consumption without and with NO addition and thus the respective interaction chemistry. This investigation firstly contributes a consistent set of temperature-dependent concentration profiles for these two butene isomers under conditions relevant for engine exhaust gases. Secondly, the observed oxidation kinetics is significantly altered with the addition of NO. Specifically, NO promotes fuel consumption and introduces for *i*-butene a low-temperature behavior featuring a negative temperature coefficient (NTC) region. The present model shows reasonable agreement with the experimental results for major products and intermediate species, and it is capable to explain the promoting effect of NO that is initiated by its contribution to the radical pool. Further, it can describe the observed NTC region for the *i*-butene/NO mixture as a result of the competition of chain propagation and chain terminating reactions that were identified by reaction flow and sensitivity analyses.



## 1. Introduction

Alkenes are important intermediates in hydrocarbon combustion and, therefore, components of exhaust gases of internal combustion engines [1]. One main decomposition product of larger alkanes is butene, which is the smallest alkene with isomers containing reactive primary and secondary allylic carbon sites. These butene isomers could interact with other exhaust gas components homogeneously. So far, propane and propene are the species of choice to account for the hydrocarbon chemistry in most studies on homogeneous gas-phase as well as heterogeneous catalytic reactions of exhaust gases, and little attention has been given to $C_4$ species. Furthermore, the kinetics of chemical conversion in exhaust gases is commonly studied at stochiometric and lean conditions, sometimes including slightly rich conditions as well. However, rich conditions may also occur in engine operation, for instance during cold start-up and regeneration of catalysts. Aside from *rich* regeneration of the well-known Lean-$NO_x$-Trap (LNT) for

* Corresponding author at: Institute for Chemical Technology and Polymer Chemistry, Karlsruhe Institute of Technology (KIT), Engesserstraße 20, 76131 Karlsruhe, Germany.
*E-mail address:* deutschmann@kit.edu (O. Deutschmann).
[1] The authors contributed equally to this work.

https://doi.org/10.1016/j.combustflame.2021.111557

the reduction of $NO_x$ emissions from lean-operated engines [2–4], several further techniques have been recently proposed to regenerate catalysts by short periods of rich engine operation to overcome water inhibition and sulphur poisoning, for instance [5–7]. Along these lines, lean-operated natural gas engines are of special interest, because, on one side, they offer high engine efficiency and less carbon dioxide emissions compared to diesel operated engines, however, on the other side, their exhaust gas aftertreatment systems suffer from rapid deactivation of the oxidation catalyst for treating the rather significant methane slip [8]. Again, short rich pulses have been shown to reactivate the catalyst [9]. The rich pulses may also be realized by injecting additional fuel into the tailpipe. The fuels can then interact with other exhaust gas components in the gas phase, calling for a better understanding of the interaction kinetics between the fuel and e.g., $NO_x$.

Furthermore, significant gas-phase reactions have recently been shown to occur at operating conditions that are characteristic for the *engine-close* part of the tailpipe of internal combustion engines [10–15]. Gas-phase reactions bear a significant impact on the catalytic conversion process, because a modified composition of the exhaust influences the appropriate performance of the catalytic converter. For instance, variations of the $NO_x/NH_3$ ratio, needed for the $NH_3$-SCR (selective catalytic reduction) of $NO_x$, may either lead to $NO_x$ or ammonia slip requiring additional measures. Consequently, special attention should be given to the understanding of gas-phase kinetics of both the decomposition chemistry of alkenes and their interaction with nitrogenous species in the low-temperature range and at diluted conditions.

In this context, the present investigation has two main aims: First, our study provides a consistent set of detailed measured species profiles for butene isomers, 1-butene and *i*-butene, at conditions relevant to exhaust gases, i.e. in the appropriate temperature range and in highly diluted mixtures under oxidative conditions. Second, the experimental results, together with a newly established model, provide the basis for a more detailed analysis of the interaction chemistry of 1-butene and *i*-butene with NO.

Previous experimental and numerical studies regarding the combustion of different $C_4$ hydrocarbon isomers are reported in the literature. With respect to the present work, they concern 1-butene oxidation and pyrolysis in different environments, such as flow reactors [16], jet-stirred reactors (JSR) [17], shock tubes [18] and counter-flow flames [19,20]. Pyrolysis and oxidation have been studied for *cis*-2-butene [20] and *trans*-2-butene [16,20–22] as well as for *i*-butene in a flow reactor [23], counter-flow flame [19], shock tube [24–27], JSR [28] and in premixed laminar flames [20,21,29]. Zhang et al. [16] have investigated the pyrolysis of three butene isomers at low pressure and 900-1900 K. Also, Fenard et al. [22] have studied the oxidation of 1-butene and *cis*-2-butene in a JSR and a combustion vessel. To the best of our knowledge, however, experimental data for the direct comparison of 1-butene and *i*-butene under exhaust-gas-relevant conditions are not yet available.

Regarding the interaction of HCs with $NO_x$, previous work has focused mainly on methane [11,15,30–40] as the main component of natural gas or gas blend [41]. Also, the combinations ethene/NO [33,42–44], propene/NO [33,43,45] as well as larger alkanes/NO [46] were studied experimentally and numerically, revealing a mutually sensitizing effect of HC and NO which can be ascribed to the interactions of $NO_x$ and the radical pool. With relevance to butene oxidation, Liu et al. [47] have recently studied the redox reactions between allyl radicals and $NO_x$. Reactions leading to allyl radicals were also observed to be very important by Prabhu et al. [48] in their investigation on interactions of 1-pentene with NO. Although detailed kinetics models [16,20,21,49] are available to simulate the oxidation of the pure fuels 1-butene and *i*-butene, a respective model for the oxidation of 1-butene/NO and *i*-butene/NO mixtures is still lacking.

In the present work, we have therefore investigated the low-temperature oxidation of 1-butene and *i*-butene without and with the addition of NO (1000 ppm) at fuel-rich conditions ($\phi = 2.0$) in a laminar flow reactor at atmospheric pressure. Concentrations of numerous species were measured in a temperature range of approximately 600-1200 K depending on the reactivity of the respective mixture; detailed information on the temperature range studied for each mixture is provided in Table 1. Synchrotron vacuum ultraviolet photoionization mass spectrometry (SVUV-PIMS) was used to obtain quantitative species profiles of oxidation products and intermediates. Note that fuel-rich conditions were predominantly investigated here since they provide more pronounced interactions between butene and NO. A detailed kinetics model was developed to simulate the reactions of the 1-butene/NO and *i*-butene/NO mixtures and to gain further insights into the butene/NO reactivity. In addition, the kinetics model was also validated against fuel-lean conditions. These results were part of a subsequent study in a different reactor setup, however, and they are thus only provided in the Supplemental Material (SM1).

## 2. Experimental method

The experiments were performed in a flow reactor apparatus at the Combustion and Flame beamline at the National Synchrotron Radiation Laboratory, China, that has been described before [50–53]. Experiments regarding the oxidation of both butenes and their combinations with added NO were performed at fuel-rich ($\phi = 2.0$) conditions under high Ar dilution and at atmospheric pressure in the temperature range of 632-1158 K (see Table 1 for details). Initial gas conditions and oven temperatures are listed in Table 1, together with abbreviations for the four cases that will be used throughout the discussion. The gas mixture, with a total flow rate of 250 standard cubic centimeters per minute (sccm), was fed into a flow reactor with 0.7 cm inner diameter and 40 cm heating length. 1-Butene (purity 99.9%), *i*-butene (purity 99.99%), NO (purity 99.99%), $O_2$ (purity 99.999%) and Ar (purity 99.999%) were purchased from Nanjing Special gases Factory Ltd., China. The flow rate of each gas was controlled by a mass flow controller (MKS, USA). To avoid the rapid conversion of NO to $NO_2$, NO and $O_2$ were guided into the reactor by separate pipes. It was determined experimentally whether NO was partially oxidized by $O_2$ under these conditions, but only NO could be detected. Therefore, the rapid conversion was found to be negligible in the present study. Depending on the reactor temperature, the average residence time in the flow reactor was between 0.6 and 1.4 s. A flow tube made of $\alpha$-alumina was used to reduce wall catalytic effects [54]. Temperature profiles along the flow tube, which are exemplarily displayed in Fig. S1 in SM1 for six setpoint temperatures of the oven, were determined for a total of 25 oven setpoints with an uncertainty of $\pm 5$ K using a S-type thermocouple following the method described earlier [50]. Previously reported methodologies for intermediate species identification and mole fraction evaluation were applied [16,51]. The uncertainties of evaluated mole fractions were estimated as $\pm 20\%$ for species with known photoionization cross sections (PICSs) and a factor of 2 for those with estimated PICSs. The respective PICSs used for quantification are provided in Table S1 and the expected species uncertainties are provided in Table S2 in SM1. Mole fractions for detected species from all above-mentioned experiments are provided in SM2 for fuel-rich conditions and in SM3 for fuel-lean conditions.

**Table 1**
Experimental conditions (mole fractions; equivalence ratio) investigated in this study.

| Gas mixture | Case | $X_{Ar}$ | $X_{C4H8}$ | $X_{O2}$ | $X_{NO}$ | $\phi$ | $T$ (K) |
|---|---|---|---|---|---|---|---|
| 1-butene/$O_2$ | 1Bu | 0.960 | 0.010 | 0.030 | – | 2.0 | 734–1011 |
| *i*-butene/$O_2$ | *i*Bu | 0.960 | 0.010 | 0.030 | – | 2.0 | 785–1158 |
| 1-butene/$O_2$/NO | 1Bu/NO | 0.959 | 0.010 | 0.030 | 0.001 | 2.0 | 632–986 |
| *i*-butene/$O_2$/NO | *i*Bu/NO | 0.959 | 0.010 | 0.030 | 0.001 | 2.0 | 632–1085 |

## 3. Kinetics modeling

The kinetics model used for the simulation and analysis of the experimental results was developed by extending our previous model devoted to propene/$NO_x$ interactions [45]. It is based on the Aramco core mechanism [55] and includes $NO_x$ chemistry from Glarborg et al. [56] and several additional sources [36,43,57–59]. The sub-mechanism describing interactions of $C_4$ species with NO and $NO_2$ was developed in this work as follows.

Several reaction classes were included in the $C_4/NO_x$ sub-mechanism, i.e., 1) H-atom abstraction reaction by $NO_2$; 2) reactions of butenyl radicals with $NO_2$; 3) reactions of butenal with $NO_2$; 4) consumption reactions of nitrobutene; 5) reactions of butenyl with NO; 6) consumption reactions of nitrosobutene and 7) reactions of butenylperoxides with NO. The H-atom abstraction reaction by $NO_2$ attack was demonstrated as an important reaction class for alkene consumption [45]. In this work, the rate coefficients for the H-atom abstraction reactions of 1-butene and *i*-butene were taken from the work of Chai and Goldsmith [57]. Further reactions of butenyl radicals with $NO_2$ can either produce butenyloxy radicals via oxidation or be stabilized to nitrobutene via recombination. Rate coefficients for the 1-buten-3-yl and *i*-butenyl radicals with $NO_2$ were taken in analogy to those for similar reactions of allyl [58]. Rate coefficients for other butenyl radicals with $NO_2$ were assumed in analogy to those for similar reactions of ethyl and vinyl [42]. The decomposition of butenyloxy radical easily produces butenal, which can induce the H-atom abstraction reaction by $NO_2$. In this work, the rate coefficients for these reactions were estimated by analogy to the similar reactions of acetaldehyde [42,56]. The decay of nitrobutene proceeds mainly through H-atom abstraction and subsequent $\beta$-scission reactions. These reactions were included in the present model with rate coefficients analogous to those for similar reactions of nitropropene [59]. The reaction of butenyl with NO mainly produces nitrosobutene via the recombination reaction, and its rate coefficient was assumed in analogy to that for the similar reaction of ethyl [42,56]. The consumption of nitrosobutene occurs mainly through unimolecular decomposition and H-atom abstraction followed by $\beta$-scission reactions. These reactions were included here with rate coefficients in analogy to the similar reactions of nitrosoethane [42,56]. The rate coefficients for the reactions of butenylperoxides with NO were analogous to those for similar reactions of propenylperoxide [59]. The nomenclature of species, selected reactions describing the $C_4H_8$–$NO_x$ interactions and thermodynamic properties of $C_4$ species in the present model are provided in Tables S3, S4 and S6 in SM1, respectively.

The thermochemical properties of nitrobutene and nitrosobutene are critical for the equilibrium. Hence, their thermodynamic properties were calculated with the CBS-QB3 method by using the Gaussian 09 program [60]. For other species in the $C_4/NO_x$ submechanism, the thermodynamic properties were estimated using THERM [61] with updated group values [62]. The reaction mechanism and thermodynamic data are provided in SM3. The simulations and kinetic analyses were performed with the Plug Flow Reactor module in the Chemkin-PRO [63] software using measured centerline temperature profiles as input parameters, which are exemplarily shown in Fig. S1 in SM1 for six setpoint temperatures of the oven.

## 4. Results and discussion

The following discussion is divided into three main sections. Section 4.1 provides an overview of the general fuel reactivity based on selected measured and simulated species profiles. A comparison of species detected in the four gas mixtures is presented in Table S4 in SM1. Unstable intermediates such as radicals were not detected under the investigated conditions. Note that the experiments were performed at photon energies between 9.5 and 14.75 eV and thus species with ionization energies above these values, such as particularly hydrogen, could not be detected in the present study. To permit visualization of the initial consumption pathways for all four cases and to highlight important structural differences, integral rate of production (ROP) analyses are given in this section at 50% fuel conversion. As a next step, Section 4.2 is then devoted to a deeper discussion of the reactions taking place in the low-temperature regime in the oxidation process of the different fuels with and without NO addition. Reactions at low temperature are of particular interest here, since a distinct NTC behavior was solely observed for the *i*Bu/NO case. It is therefore of crucial importance to identify the reactions that lead to the observed differences. The combustion reactions between the four cases, based on the oxidation of pure 1Bu and *i*Bu (Section 4.2.1) are thus first analyzed with a focus on species in the H,C,O system, together with a sensitivity analysis regarding important reactions for the two fuel isomers. Finally, Section 4.2.2 focuses on the impact of NO addition on the oxidation and HC/NO interaction chemistry of 1Bu and *i*Bu. Mole fraction profiles are presented for some representative nitrogen-containing species, complemented by sensitivity analyses for the butene/NO mixtures. Specifically, nitrogenous intermediates detected and identified in this work include hydrogen cyanide (HCN), nitrous acid (HONO), nitromethane ($CH_3NO_2$), 3-nitroso-2-methyl-1-propene ($IC_4H_7NO$) and 3-nitro-2-methyl-1-propene ($IC_4H_7NO_2$). Throughout the discussion in all sections, the information from experimental and simulated species profiles as well as from the ROP and sensitivity analyses are combined to gain deeper insight into the relevant oxidation chemistry. The interaction effects with NO are analyzed along the reaction paths considering the determined species profiles to better understand the outcome of reactions in exhaust gases that might lead to undesirable or even toxic emissions.

### 4.1. Fuel reactivity and initial fuel consumption reactions

To start the comparison of the fuel reactivity for the four cases, Fig. 1 shows experimental and simulated mole fraction profiles of several species, i.e., butene, CO, NO and $NO_2$. The profiles of butene are depicted to represent the fuel consumption, while CO is selected as an important conversion product under fuel-rich conditions. NO as well as $NO_2$ are included to show their involvement in the reaction process.

For the mole fraction profiles of the two butenes and CO, which are shown in Fig. 1a-b, reasonable agreement between experiment

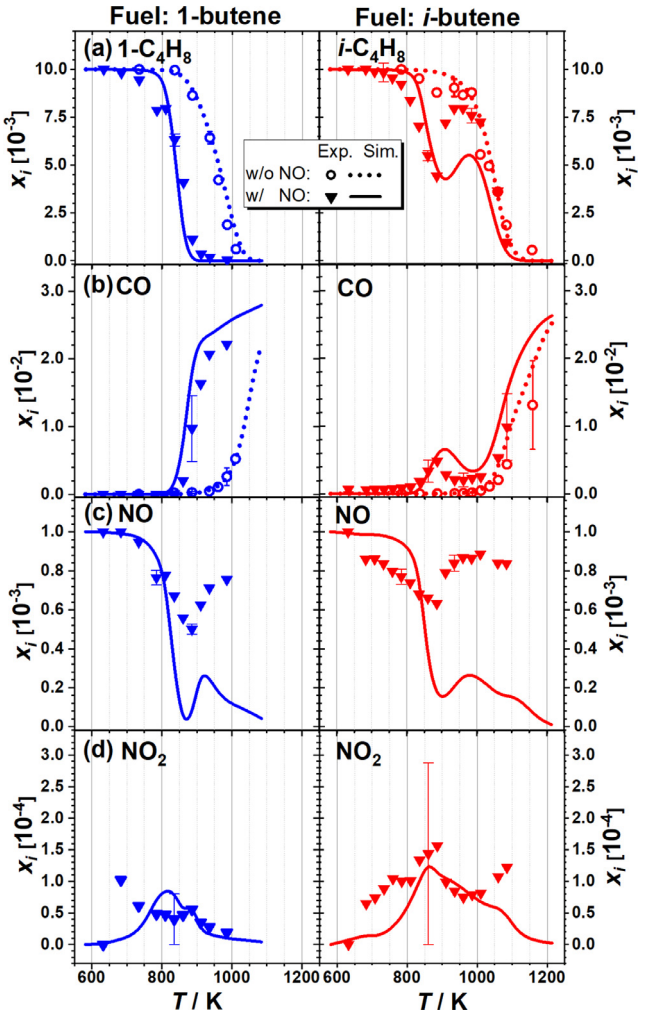


**Fig. 1.** Experimental and simulated mole fractions of (a) fuel (1-$C_4H_8$, *i*-$C_4H_8$), (b) CO, (c) NO, (d) $NO_2$ in the oxidation of 1Bu (left) and *i*Bu (right) without NO (Exp: circle, Sim: dotted line) and with NO (Exp: square, Sim.: solid line) as a function of temperature. For clarity, experimental uncertainties are only indicated as error bars (bold: w/ NO, normal: w/o NO) at selected temperatures.

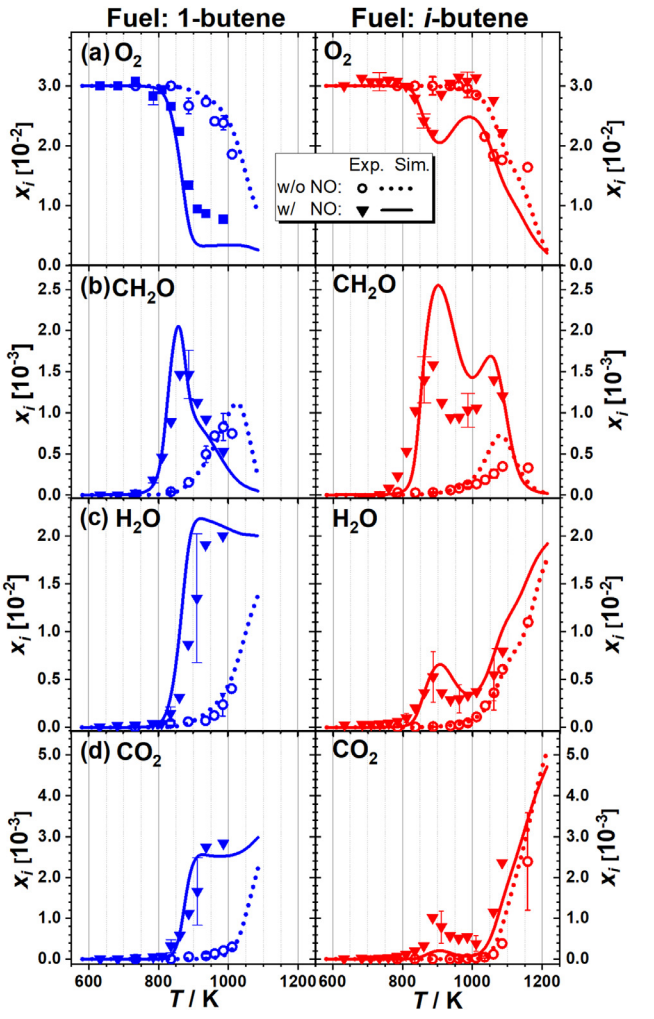


**Fig. 2.** Experimental and simulated mole fractions of (a) $O_2$ (b) $CH_2O$, (c) $H_2O$, (d) $CO_2$ in the oxidation of 1Bu (left) and *i*Bu (right) without NO (Exp: circle, Sim: dotted line) and with NO (Exp: square, Sim: solid line) as a function of temperature. For clarity, experimental uncertainties are only indicated as error bars (bold: w/ NO, normal: w/o NO) at selected temperatures.

and modeling results is observed, while an over-predicted consumption between 900 K and 1100 K can be seen for the mole fraction profiles of NO, shown in Fig. 1c, for both fuel/NO mixtures. For the mole fraction profiles of $NO_2$, provided in Fig. 1d, deviations between experiment and modeling can be noticed, which are still within the experimental uncertainty. For fuel profiles of 1Bu and *i*Bu in Fig. 1a, onset temperatures of 890 K and 990 K are observed, respectively, while these are shifted about 80 K towards lower temperatures when NO is added. The most striking feature is the observed negative temperature coefficient (NTC) behavior that is only seen for the *i*Bu/NO case. Also, for pure *i*Bu, slightly lower fuel mole fractions, which are still within the experimental uncertainty, are observed in the temperature range of 900–1000 K. However, this observation cannot be traced back to a weak NTC behavior since neither $O_2$ is consumed nor is $CH_2O$, which is a well-known indicator for low-temperature reactivity, formed in the respective temperature range as can be seen in Fig. 2a-b.

In general, NTC behavior as known for the low-temperature oxidation of hydrocarbons can be explained by the competition of reactions accelerating or inhibiting the reactivity dependent on temperature [46]. A similar effect upon NO addition was observed in our recent study on propene/$NO_x$ [45]. At total fuel consumption, a different behavior between the neat 1Bu and *i*Bu as well as the mixtures with NO addition is again observed. In the 1Bu/NO case, the addition of NO shifts the total 1Bu consumption about 150 K towards lower temperatures, corresponding to a promoting effect of NO on 1Bu reactivity. In contrast, the NO addition in the *i*Bu/NO case does not lead to an earlier total consumption of *i*Bu. Reasonable agreement between experiment and model, regarding both peak mole fraction and profile shape, is observed in all four cases for the mole fraction profiles of the fuel. The trend of the NTC region for the *i*Bu/NO mixture can be satisfactorily represented by the model, although it over-predicts the fuel consumption between 900 K and 1000 K. The experimental mole fraction profiles of CO (Fig. 1b) are also captured with good agreement, especially of the measured profile shapes, by the simulation results. For the mole fraction profiles of NO and $NO_2$ (Fig. 1c and d), the proposed model over-predicts the NO consumption between 900 K and 1100 K for both fuel/NO mixtures. The consumption and formation of NO are related to complex reaction sequences, including both reactions in the $C_4/NO_x$ sub-model and the reaction in the base $NO_x$ model. In the present work, the over-prediction of the NO consumption rate may come from the uncertainties in the kinetic reaction parameters developed in this paper for the $C_4/NO_x$ sub-model (as discussed in Section 4.2.2) and maybe also from some uncertainties in the base $NO_x$ model. Therefore, further comprehensive experi-

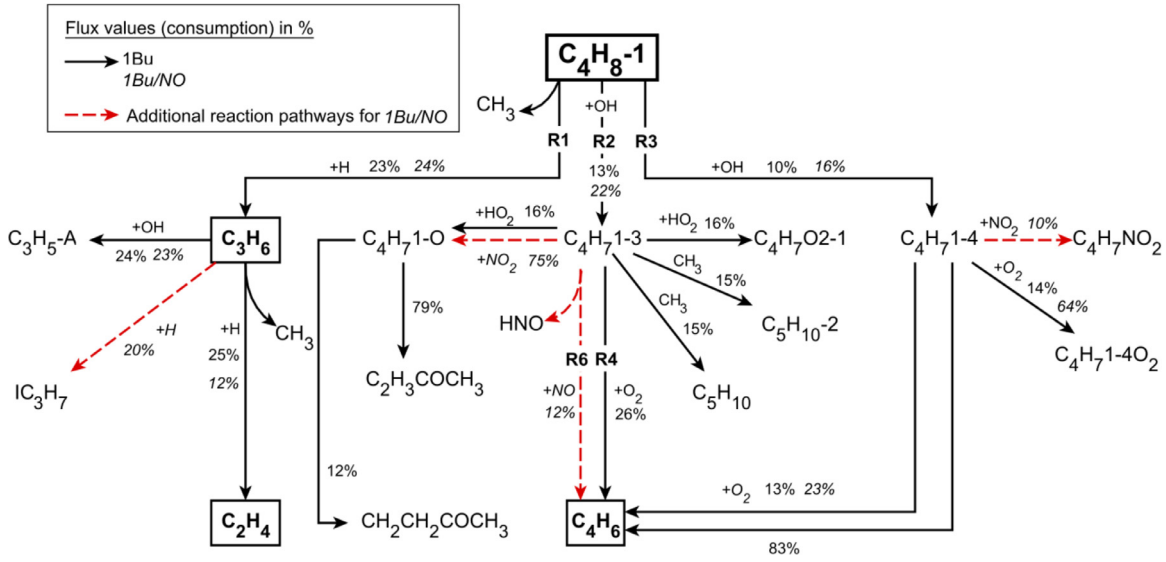


**Fig. 3.** Major consumption pathways with contributions >10% in the oxidation of 1Bu without (regular letters, solid arrows) and with NO (italic letters, solid arrows as well as additional pathways due to NO addition with (red) dashed arrows) at 50% fuel conversion at 962 K and 838 K, respectively, based on integrated flows. Mole fraction profiles are provided for species highlighted with boxes, and the nomenclature is according to the kinetics model (see Table S3 in SM1).

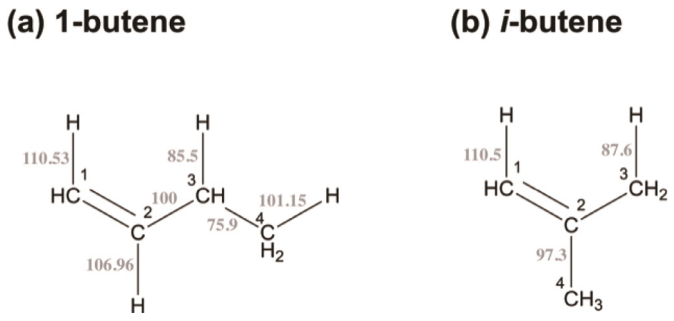


**Fig. 4.** Bond dissociation energies (in kcal/mol) of 1Bu and *i*Bu. C–H bond dissociation energies of 1Bu were taken from [49]; C–C bond dissociation energies of 1Bu were taken from [64]. Bond dissociation energies of *i*Bu were taken from [65].

mental and theoretical studies are recommended for this chemical system.

For better insight into the reactions causing the differences in the fuel reactivities, ROP analyses were performed at 50% fuel conversion for the four cases. Only the initial fuel consumption steps are shown for each case for clarity.

Under the present conditions, 1Bu oxidation is initiated by three main reactions, R1–R3:

$$C_4H_8\text{-}1 + H = C_3H_6 + CH_3 \quad (R1)$$

$$C_4H_8\text{-}1 + OH = C_4H_7\text{1-}3 + H_2O \quad (R2)$$

$$C_4H_8\text{-}1 + OH = C_4H_7\text{1-}4 + H_2O \quad (R3)$$

According to the ROP analysis in Fig. 3, the most important consumption pathway is the decomposition via reaction R1 forming propene ($C_3H_6$) with contributions of 23% and 24% for the 1Bu and 1Bu/NO case. This dominant influence is due to the low C–C bond energy between the carbon atoms at positions 3 and 4; structures and bond energies for both isomers are provided in Fig. 4.

This observation is also in agreement with the butene flame study of Schenk et al. [21], who have also identified this reaction as the major decomposition pathway for 1Bu, *trans*-2-butene and 2-butene. At 50% fuel conversion, $C_3H_6$ is mainly produced with 84% in the 1Bu oxidation according to the ROP analysis. As the initial decomposition product, $C_3H_6$ further reacts, forming $C_3H_5$-A and $C_2H_4$. The mole fraction profiles of the two stable intermediates, $C_3H_6$ and $C_2H_4$ that are both formed via initial decomposition steps are provided in Fig. 5a-b. $CH_4$ and $C_4H_6$, also presented in Fig. 5 so that respective profile shapes can be compared, are discussed further below, following the main reaction sequences.

Following the ROP analysis, the H-abstraction reactions R2 and R3 at the carbon positions $C_3$ and $C_4$, forming 1-methyl-2-propenyl ($C_4H_7$1-3) and but-3-en-1-yl ($C_4H_7$1-4) radicals, are with 13% and 10% (1Bu), respectively, the second and third most important consumption reaction in the oxidation of the 1Bu and 1Bu/NO mixture due to the comparatively weak C–H bonds (see Fig. 4a). In contrast, the H-abstraction reactions at carbon positions $C_1$ and $C_2$ are unfavored due to larger bond energies of 110.53 kcal/mol and 106.96 kcal/mol, respectively, and the formation of $C_4H_7$1-2 and $C_4H_7$1-1 radicals is therefore less important [22].

The main consumption pathway of the $C_4H_7$1-3 radicals in the 1Bu oxidation is via reaction R4 forming $C_4H_6$ (see Fig. 5d) and $HO_2$ radicals. The unreactive $HO_2$ radicals are converted into reactive OH radicals by reaction R5. The OH radicals are then needed for the initial fuel consumption reactions R2 and R3 and thus the OH radicals increase the fuel reactivity. Reaction R5 is the main source of the OH radicals in the neat fuel oxidation at 50% conversion.

$$C_4H_7\text{1-}3 + O_2 = C_4H_6 + HO_2 \quad (R4)$$

$$CH_3 + HO_2 = CH_3O + OH \quad (R5)$$

Important for the low-temperature reactivity is the formation of the oxygenated species, such as $C_4H_7$1–O, $C_4H_7O_2$-1, which are chain-branching and thus increase the fuel reactivity. During the formation of the oxygenated species, $HO_2$ radicals are again released and converted into reactive OH radicals.

Most of the reaction pathways in the 1Bu/NO mixture are similar to those of the neat 1Bu oxidation. However, as obvious from fuel profiles in Fig. 1a, the reactivity in the 1Bu/NO mixture is higher compared to that of the neat fuel. This can be explained by additional reaction pathways due to the NO addition in the mixture. Reaction R6 contributes with 75% to the consumption of the

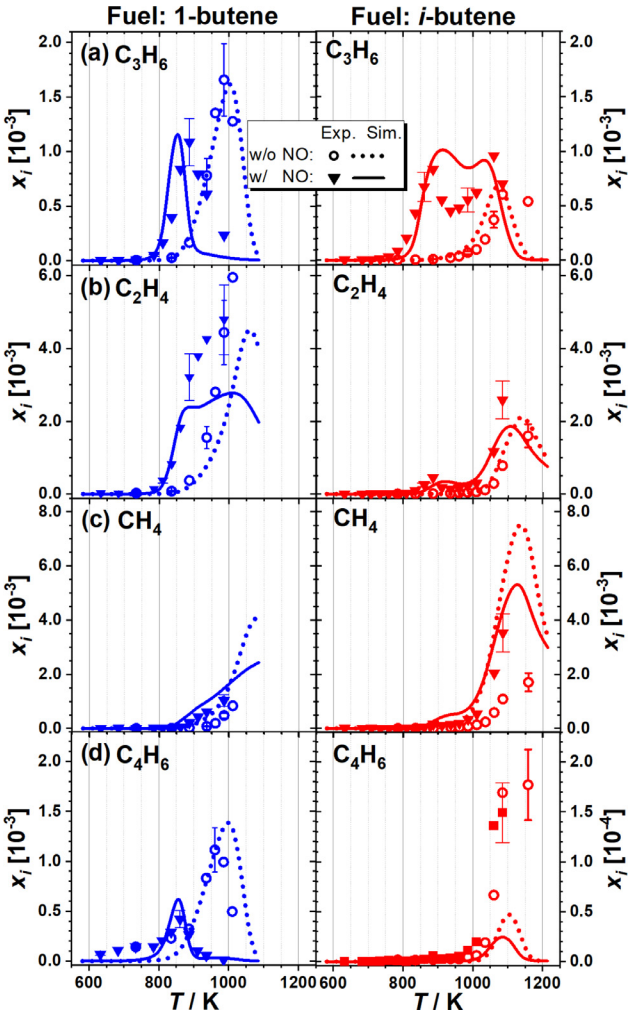


**Fig. 5.** Experimental and simulated mole fractions of (a) $C_3H_6$, (b) $C_2H_4$, (c) $CH_4$, (d) $C_4H_6$ in the oxidation of 1Bu (left) and *i*Bu (right) without NO (Exp: circle, Sim: dotted line) and with NO (Exp: square, Sim: solid line) as a function of temperature. For clarity, experimental uncertainties are only indicated as error bars (bold: w/ NO, normal: w/o NO) at selected temperatures.

$C_4H_71$-3 radical in the 1-Bu/NO case.

$$C_4H_71\text{-}3 + NO_2 = C_4H_71\text{-}O + NO \quad (R6)$$

$$NO + HO_2 = NO_2 + OH \quad (R7)$$

The formation and thus the reaction sequence significantly increase the reactivity by producing NO as well as the oxygenated species $C_4H_71$-O, which is again chain-branching. In contrast, the similar reaction sequence in the neat 1Bu oxidation, where the $C_3H_71$-3 radical reacts with $HO_2$ radicals, only contributes to the $C_4H_71$-3 radical consumption with 16%. Furthermore, the released NO reacts with unreactive $HO_2$ radicals, producing $NO_2$ and reactive OH radicals via reaction R7. This so-called interchanging reaction, which is the main source of OH radicals during the oxidation of the 1Bu/NO mixture, significantly increases the reactivity of the respective system compared to the neat 1Bu case. This promoting effect of NO on the HC oxidation is in accordance with the literature [33,39,46].

In Fig. 6, the ROP analyses of the neat *i*Bu and the *i*Bu/NO mixtures are shown. Because of the branched molecular structure of *i*Bu, its main consumption reactions differ significantly from the previously discussed consumption pathways of 1Bu. In general, the fuel reactivity is lower for the branched molecule, which is in accord with previous studies [65]. This can be traced back to the fact that its C–C and C–H bond dissociation energies, which are shown in Fig. 4b, are generally slightly higher than those of 1Bu. In the *i*Bu oxidation, the first consumption step is the radical-initiated H-abstraction reaction towards the resonance-stabilized 2-methylallyl radical ($IC_4H_7$). The formation of the $IC_4H_7$ radical is favored due to the lowest bond dissociation energy of the C–H bond at carbon position 3 (87.6 kcal/mol, see Fig. 4b) as well as the high statistical probability. For neat *i*Bu the $IC_4H_7$ radical is with 31% and 28% dominantly formed via reactions R8 and R9, respectively:

$$IC_4H_8 + CH_3 = IC_4H_7 + CH_4 \quad (R8)$$

$$IC_4H_8 + OH = IC_4H_7 + H_2O \quad (R9)$$

As a consequence, twice as much methane ($CH_4$) is produced during the oxidation of *i*Bu compared to 1Bu due to the significant importance of reaction R8 as shown in Fig. 5c. While the formation of $C_3H_6$ is of significant importance in the 1Bu and 1Bu/NO oxidation, as discussed before, this species is only of minor importance in the *i*Bu oxidation because of its molecular structure and the related favored fuel radicals. In the neat *i*Bu oxidation, $IC_4H_7$ radicals further react via the chain-propagating reaction R10 that leads to the formation of allene ($C_3H_4$-A):

$$IC_4H_7 = C_3H_4\text{-}A + CH_3 \quad (R10)$$

In Fig. 7 the mole fraction profile of $C_3H_4$-A is shown, together with the profiles of propyne ($C_3H_4$-P) and $C_2H_2$ as further observed stable intermediates. The mole fraction profiles are discussed in detail in the following sections. Reaction R10 releases important $CH_3$ radicals, which are necessary for the conversion of $HO_2$ radicals into reactive OH radicals via reaction R5, and therefore R10 also contributes to the reactivity of the *i*Bu system.

Moreover, also reaction R11 promotes the system's reactivity because $HO_2$ radicals are converted to reactive OH radicals. This reaction was also found to increase the fuel reactivity and is in accordance with the recent results of Zhou et al. [65] who studied the oxidation of *i*Bu extensively at fuel-lean and fuel-rich conditions.

$$IC_4H_7 + HO_2 = IC_4H_7O + OH \quad (R11)$$

The $IC_4H_7O$ radical decomposes quickly to methacrolein ($IC_3H_5CHO$), which is further oxidized forming $IC_3H_5CO$. The latter species decomposes to $C_3H_5$-T and finally to CO, which significantly promotes the reactivity.

As already observed for the *i*Bu case, the fuel consumption during the *i*Bu/NO oxidation also occurs mainly via reaction R9 forming the $IC_4H_7$ fuel radical. Upon addition of NO, the further reactions of this fuel radical differ considerably from those observed for the neat *i*Bu oxidation since nitrogenous reactants such as $NO_2$, are involved. In particular, the $IC_4H_7$ radical further reacts with $NO_2$ leading to the oxygenated species $IC_4H_7O$ (reaction R12).

$$IC_4H_7 + NO_2 = IC_4H_7O + NO \quad (R12)$$

While the formation of the $IC_4H_7O$ radical is chain-propagating, the formation of NO contributes again to the OH radical pool via R7 and thus to the overall reactivity of the *i*Bu/NO system. The $IC_4H_7O$ radicals further decompose quickly to $IC_3H_5CHO$ (methacrolein). The decomposition reaction of $IC_3H_5CHO$ by H-abstraction to $IC_3H_5CO$ can be observed in the *i*Bu and *i*Bu/NO oxidation, making this pathway a reactive chain sequence that is believed to be an important contributor to the low-temperature reactivity of the *i*Bu/NO mixture. In contrast to the *i*Bu oxidation, the addition of NO opens up further reaction pathways, in particular reaction R12 which contributes with 77% to the $IC_4H_7$ radical

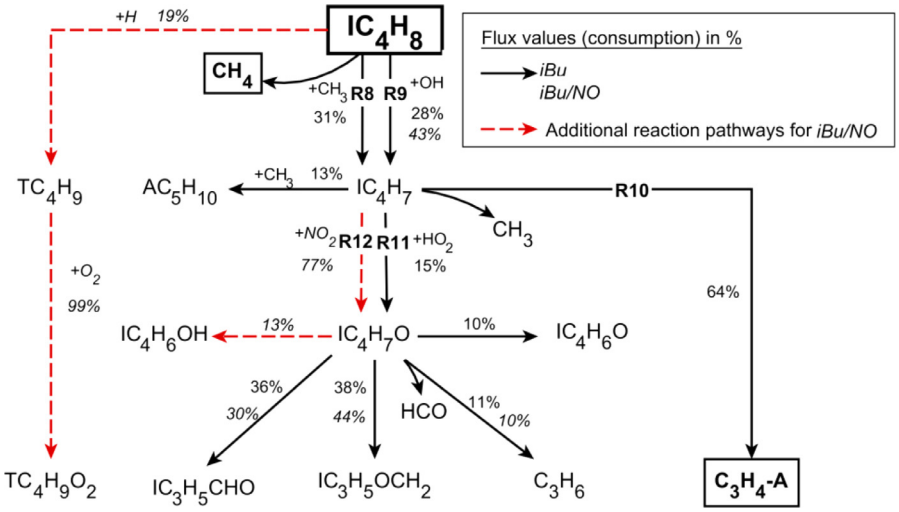


**Fig. 6.** Major consumption pathways with contributions >10% in the oxidation of *i*Bu without (regular letters, solid arrows) and with NO (italic letters, solid arrows as well as additional pathways due to NO addition with (red) dashed arrows) at 50% fuel conversion at 1043 K and 880 K, respectively, based on integrated flows. Mole fraction profiles are provided for species highlighted with boxes and the nomenclature is according to the kinetics model (see Table S3 in SM1).

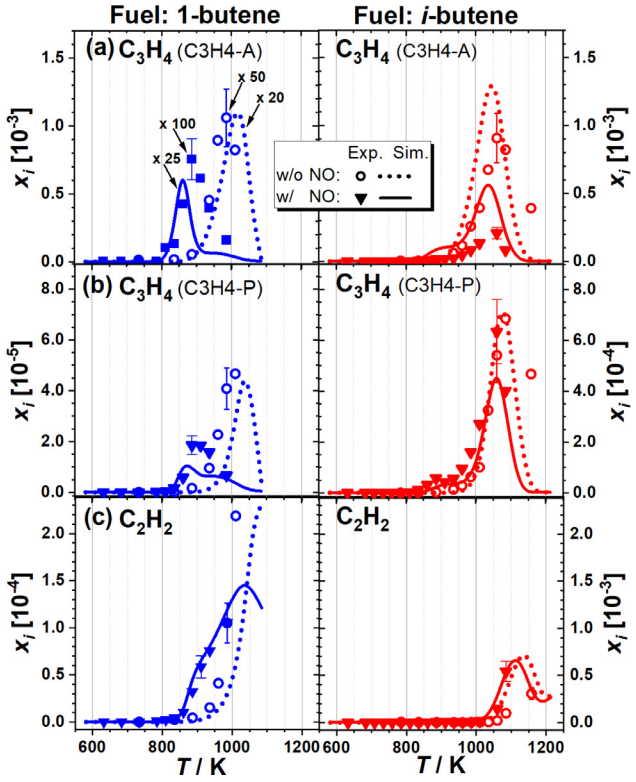


**Fig. 7.** Experimental and simulated mole fractions of (a) $C_3H_4$-A (b) $C_3H_4$-P and (c) $C_2H_2$ in the oxidation of 1Bu (left) and *i*Bu (right) without NO (Exp: circle, Sim: dotted line) and with NO (Exp: square, Sim: solid line) as a function of temperature. For clarity, experimental uncertainties are only indicated as error bars (bold: w/ NO, normal: w/o NO) at selected temperatures.

consumption, contributing thus to a chain-propagating reaction sequence that significantly increases the fuel reactivity in the *i*Bu/NO mixture.

Overall, the discussion within this section concerning the fuel reactivity at 50% conversion has shown that the differences in the fuel reactivity are mainly related to differences in the bond dissociation energies of the linear and branched fuel molecules. Thus, the observed differences between the four cases for the mole fraction profiles shown in Figs. 1 and 2 as well as the ROP analyses in Figs. 3 and 6 could mostly be explained by structural differences and therefore differences in the main reaction sequences of both neat fuels, which show important reactivity mainly in the higher temperature region above 900 K. The observed trends were reasonably captured by the present model, and differences in the mole fraction maxima could be understood in terms of the dominant reactions. The addition of NO to both fuels increases the reactivity significantly due to additional reaction pathways contributing to the radical pool.

### 4.2. Fuel-specific interaction kinetics

In the previous section it was discussed that notable differences are observed for the reactivity of the four cases. Significant differences have become obvious for the NTC region, since a distinct NTC behavior was only observed for the branched alkene doped with NO (*i*Bu/NO). The following discussion, which is based on the experimental results and the results of the newly developed model, aims to provide explanations for the observed differences within the low-temperature reaction behavior. To this end, it is of particular interest to understand the effect of NO addition and to examine the differences between 1Bu and *i*Bu oxidation in more detail, concentrating first on the reaction behavior of the two neat fuels in Section 4.2.1 and then focusing on the two cases with NO in Section 4.2.2.

To follow not only the fuel decomposition but to reveal the main differences in the further fuel-specific reaction sequences, integral ROP analyses for the four cases were also performed at the temperatures of the respective $CH_2O$ maxima. These temperatures, that somewhat differ from those of 50% fuel conversion discussed before, especially for the neat fuels, were selected to enable a comparative analysis especially in the low-temperature regime, recognizing that the $CH_2O$ maxima appropriately reflect the aforementioned temperature shifts. The results, which are illustrated for the major reaction pathways in Fig. 8 for the 1Bu and 1Bu/NO as well as in Fig. 9 for the *i*Bu and *i*Bu/NO cases, will be used for the remainder of this discussion.

To facilitate following the subsequent discussion, an overview of selected relevant reactions with their kinetic parameters is provided in Table 2.

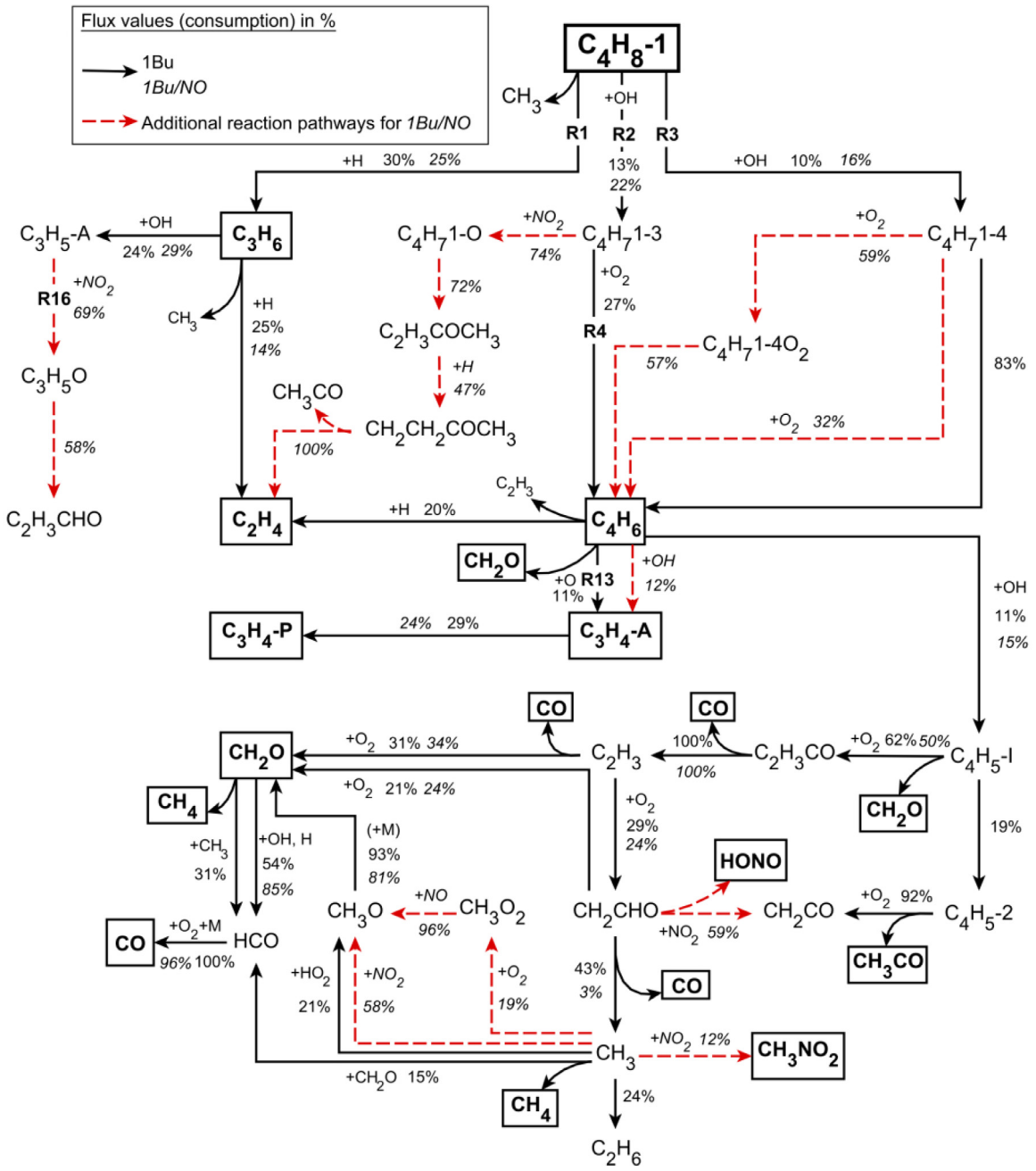


**Fig. 8.** Major consumption pathways with contributions >10% in the oxidation of 1Bu with (italic letters, solid and dashed arrows) and without NO (regular letters, solid arrows) at the temperatures of the $CH_2O$ maxima at 860 K and 1035 K, respectively, based on integrated flows (%). Mole fraction profiles are provided for species highlighted with boxes and the nomenclature is according to the kinetic model (see Table S3 in SM1).

*4.2.1. 1-Butene and* i*-Butene oxidation without NO*

With regard to the different molecular structure of both fuels, already the reactions to the first fuel radicals open up different pathways, as mentioned before. These reaction sequences will be discussed in more detail for the present conditions for 1Bu and *i*Bu. Common detected intermediates and products, although in different proportions from somewhat different reaction sequences, include CO and $CH_2O$, which were already presented in Figs. 1b and 2b, as well as $C_3H_6$, $C_2H_4$, and $C_4H_6$ shown in Fig. 5 and allene ($C_3H_4$-A) in Fig. 7a. All figures include also the profiles that were obtained for the cases with NO addition to highlight the respective changes. Note, however, that specific reactions of the 1Bu/NO and *i*Bu/NO systems will be discussed later in Section 4.2.2. For better comparison with the reaction schemes in Figs. 8 and 9, we will use species abbreviations from the kinetics model (compare Table S3 in SM1).

*1-Butene oxidation.* As already discussed in Section 4.1 at 50% fuel conversion, 1Bu oxidation is initiated by the three main reactions R1, R2 and R3 (Table 2). Again, these three reactions were also found to be the major reaction pathways at the $CH_2O$ peak temperature, as shown in Fig. 8. Propene is formed with a contribution of 30% via reaction R1. For 1Bu oxidation, $C_3H_6$ is only present in significant mole fractions above 900 K, as evident from the profiles shown in Fig. 5a. Although the cases for neat *i*Bu and for the mixtures of both fuels with NO will be discussed sequentially below, it may be useful to keep in mind that all $C_3H_6$ profiles are reasonably well captured by the kinetics model.

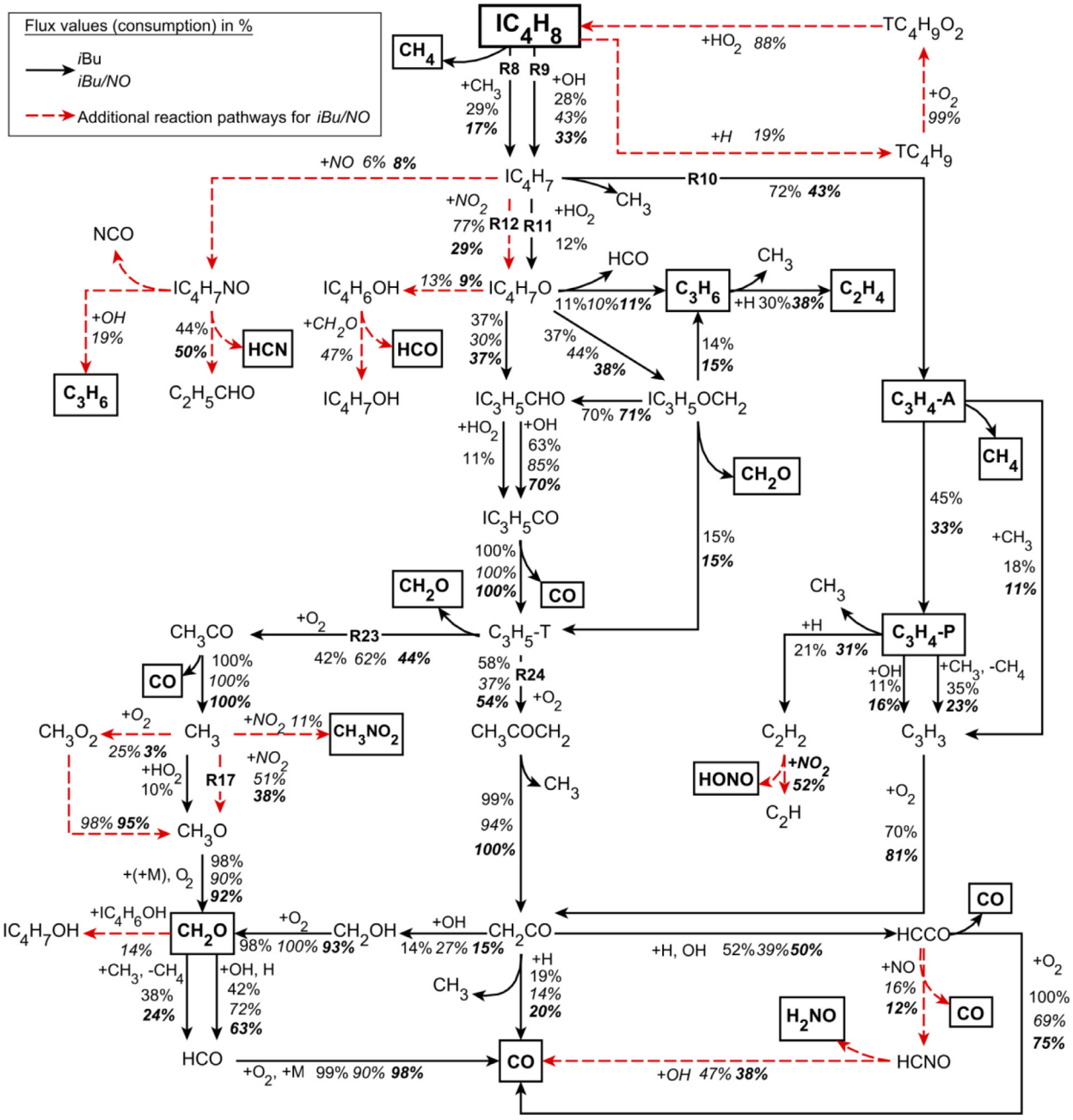


**Fig. 9.** Major consumption pathways (>10%) in the oxidation of *i*Bu with (italic letters, solid and dashed arrows) and without NO (regular letters, solid arrows) at the temperatures of the $CH_2O$ maxima based on integrated flows (%). Note that for *i*Bu/NO, the ROP was performed at 886 K (italic letters) and 1060 K (bold italic letters) since two maxima were observed upon NO addition, while a temperature of 1085 K was chosen for pure *i*Bu (see Fig. 1b). Mole fraction profiles are provided for species highlighted with boxes and the nomenclature is according to the kinetic model (see Table S3 in SM1).

Propene reacts with nearly equal probability to the resonance-stabilized allyl radical ($C_3H_5$-A) and ethylene ($C_2H_4$). Both species are with 89% and 87%, respectively, predominantly formed from $C_3H_6$ and reach their mole fraction maxima near the $CH_2O$ peak temperature. According to the ROP analysis, only a small part of $C_3H_5$-A is consumed via the reaction sequence $C_3H_5$-A→$C_3H_5O$→$C_2H_3CHO$→$C_2H_3CO$→$C_2H_3$→$CH_2O$→HCO→CO. This observation is in agreement with the results of our previous propene/$NO_x$ study [45]. Reactions of the $C_3H_5$-A radical are of noticeable influence on the reactivity, as seen in the sensitivity analysis in Fig. 10a.

While its formation reaction decreases the reactivity, the consumption reaction of the $C_3H_5$-A radical with $HO_2$ forming $C_3H_5O$ (as the first step in the aforementioned reaction sequence) increases the reactivity at the $CH_2O$ peak temperature.

Whereas the quantification of the $C_3H_5$-A radical was not possible in the present experiment, $C_2H_4$ was experimentally detected and its mole fraction profile was shown in Fig. 5b, Section 4.1. The trends seen in the experiment are reasonably well captured by the model although it predicts the maximum for neat 1Bu at a slightly higher temperature than observed in the experiment. Ethylene is consumed via the reaction sequence $C_2H_4$→$C_2H_3$→$CH_2O$→HCO→CO. Both aforementioned reaction routes, namely the consumption of $C_3H_5$-A radical and $C_2H_4$, lead to the formation of CO and $CH_2O$. Since 1Bu consumption occurs predominantly above 900 K, $CH_2O$ must be considered rather

**Table 2**
Reactions mentioned within the discussion with kinetics parameter. Rate coefficients are given as $k = AT^{\beta}\exp(-E_a/RT)$ (*A*: cm/s/K/mol; *Ea*: cal/mol); R1: $k = k_1 + k_2$.

| | Reaction | *A* | *ß* | *Ea* | Reference |
|---|---|---|---|---|---|
| R1 | $C_4H_8$-1+H=$C_3H_6$+$CH_3$ | 4.57E19 | −1.54 | 9061.0 | [55] |
| | | 1.21E16 | −0.99 | 13,170.0 | |
| R2 | $C_4H_8$-1+OH=$C_4H_7$1-3 + $H_2O$ | 4.14E04 | 2.55 | −1742.0 | [55] |
| R3 | $C_4H_8$-1+OH=$C_4H_7$1-4 + $H_2O$ | 2.51E05 | 2.28 | −1209.0 | [55] |
| R4 | $C_4H_7$1-3 + $O_2$=$C_4H_6$+$HO_2$ | 4.88E01 | 3.48 | 34,800.0 | [55] |
| R5 | $CH_3$+$HO_2$=$CH_3O$+OH | 1.00E12 | 0.27 | 688.0 | [55] |
| R6 | $C_4H_7$1-3+$NO_2$=$C_4H_7$1-*O*+NO | 1.65E17 | −1.55 | 0.0 | [58] |
| R7 | NO+$HO_2$=$NO_2$+OH | 2.10E12 | 0.00 | −497.0 | [56] |
| R8 | $IC_4H_8$+$CH_3$=$IC_4H_7$+$CH_4$ | 3.20E12 | 0.00 | 10,000.0 | [55] |
| R9 | $IC_4H_8$+OH=$IC_4H_7$+$H_2O$ | 1.01E07 | 2.00 | 200.0 | [66] |
| R10 | $IC_4H_7$=$C_3H_4$-*A*+$CH_3$ | 7.10E10 | 1.38 | 56,360.0 | [67] |
| R11 | $IC_4H_7$+$HO_2$=$IC_4H_7O$+OH | 7.77E17 | −1.52 | 2379.0 | [55] |
| R12 | $IC_4H_7$+$NO_2$=$IC_4H_7O$+NO | 1.65E17 | −1.55 | 0.0 | [58] |
| R13 | $C_4H_6$+O=$CH_2O$+$C_3H_4$-A | 7.26E10 | 0.82 | 1829.0 | [55] |
| R14 | $O_2$+H=O+OH | 1.04E14 | 0.00 | 15,200.0 | [55] |
| R15 | $HO_2CH_2CO$=>CO+$CH_2O$+OH | 2.51E19 | −2.95 | 8110.0 | [55] |
| R16 | $C_3H_5$-A+$NO_2$=$C_3H_5O$+NO | 1.65E17 | −1.55 | 0.0 | [58] |
| R17 | $CH_3$+$NO_2$=$CH_3O$+NO | 1.10E13 | 0.00 | 0.0 | [56] |
| R18 | $CH_2CHO$+NO=HCN+HOCHO | 7.00E21 | −3.38 | 1025.0 | [56] |
| R19 | $C_2H_3$+NO=HCN+$CH_2O$ | 4.00E13 | −0.20 | 0.0 | [56] |
| R20 | $IC_4H_8$+$O_2$=$IC_4H_7$+$HO_2$ | 3.12E13 | 0.00 | 37,400.0 | [55] |
| R21 | $IC_4H_7$+$IC_4H_7$=H15DE25DM | 1.00E11 | 0.00 | 0.0 | [55] |
| R22 | HNO+$NO_2$=HONO+NO | 4.40E04 | 2.64 | 4040.0 | [56] |
| R23 | $C_3H_5$-T+$O_2$=$CH_3CO$+$CH_2O$ | 2.55E20 | −2.61 | 1566.0 | [55] |
| R24 | C3H5-T+O2=CH3COCH2+O | 9.86E25 | −3.75 | 11,255.0 | [55] |

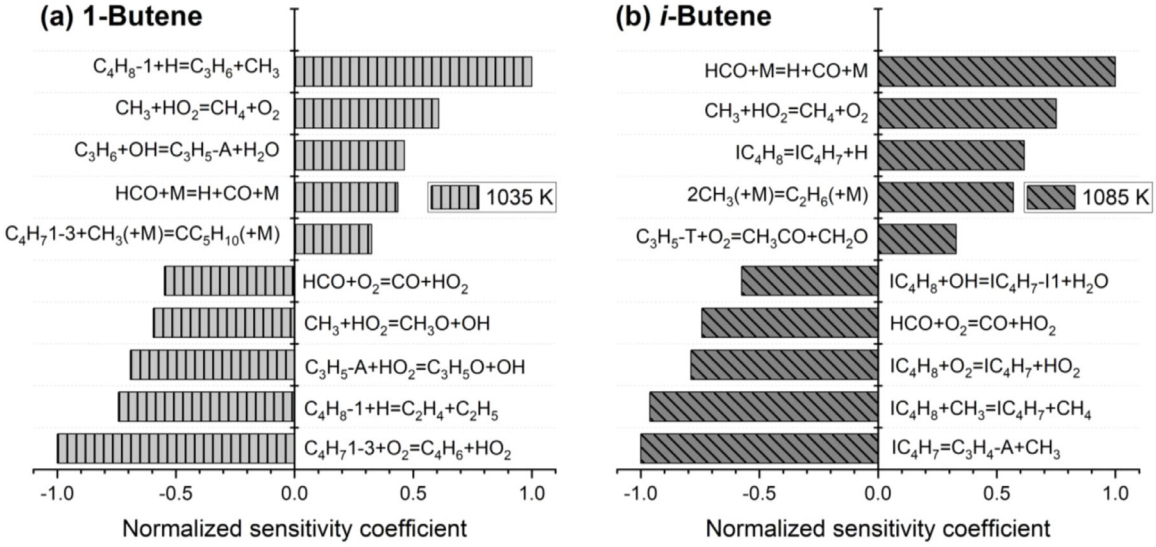


**Fig. 10.** Sensitivity analyses for neat (a) 1Bu and (b) *i*Bu at the respective $CH_2O$ peak temperature at 1035 K (99% fuel conversion) and 1085 K (87%). Reactions represented with a negative normalized sensitivity coefficient enhance fuel consumption, while reactions represented with a positive normalized sensitivity coefficient inhibit the reactivity instead.

as a product in the oxidation sequence and not as an indicator for low-temperature chemistry.

In the 1Bu oxidation under the present conditions, $C_4H_7$1-3 radical is with 13% the second most important fuel radical (compare Fig. 8) formed via reaction R2. Its main consumption pathway is the oxidation reaction R4 forming $C_4H_6$ and $HO_2$. As discussed in Section 4.1, this reaction increases the reactivity via reaction R5. Reaction R4 was also found to be the most sensitive reaction according to the sensitivity analysis shown in Fig. 10a, confirming the described observation.

The third 1Bu oxidation pathway occurs via $C_4H_7$1-4 radicals formed via reaction R3 (compare Fig. 8). These are with 83% predominantly consumed in the reactions towards $C_4H_6$, whose mole fraction profile was shown in Fig. 5d as a sum of all $C_4H_6$ isomers. The model again predicts a maximum for the 1Bu case at slightly higher temperatures than seen in the experiment. $C_4H_6$ mainly decomposes to $C_2H_4$ and $C_2H_3$. Other reaction pathways such as $C_4H_6$+O=$CH_2O$+$C_3H_4$-A are also relevant for $C_4H_6$ decomposition, even though their contribution is of less importance with 11%. The formation of the stable molecules $CH_2O$ and $C_3H_4$-A decreases the reactivity of the system. Allene further converts to propyne ($C_3H_4$-P) by H-atom catalyzed isomerization. Both $C_3H_4$ isomers, $C_3H_4$-A and $C_3H_4$-P, were experimentally observed and their mole fraction profiles are presented in Fig. 7a-b. The measured species mole fraction profiles reveal that the formation of $C_3H_4$-A and $C_3H_4$-P is favored at temperatures above 1000 K as predicted correctly by the kinetics model. Consecutive reactions of propyne result in the formation of either propargyl ($C_3H_3$) and $CH_4$ or acetylene ($C_2H_2$) and $CH_3$. Both $CH_4$ and $C_2H_2$ were experimentally detected, and their mole fraction profiles are included in Figs. 5c and 7c.

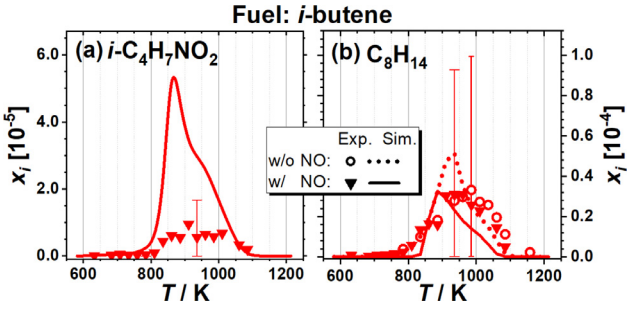


**Fig. 11.** Experimental and simulated mole fractions of (a) $i$-$C_4H_7NO_2$ and (b) $C_8H_{14}$ in the oxidation of *i*Bu without NO (Exp: circle, Sim: dotted line) and with NO (Exp: square, Sim: solid line) as a function of temperature. For clarity, experimental uncertainties are only indicated as error bars (bold: w/ NO, normal: w/o NO) at selected temperatures.

i-*Butene oxidation.* Because of the branched molecular structure of *i*Bu, its main consumption reactions differ from the previously discussed consumption pathways of 1Bu. In general, the fuel reactivity is lower for the branched molecule because of its higher bond dissociation energy, as discussed previously in Section 4.1. In the *i*Bu oxidation, the first consumption step is the radical-initiated H-abstraction reaction towards the resonance stabilized 2-methylallyl radical ($IC_4H_7$). It is dominantly formed via reactions R8 and R9. While the formation of $C_3H_6$ is of significant importance in the 1Bu oxidation as explained previously, this species is only of minor importance in the *i*Bu oxidation because of the fuel's molecular structure and the related favored fuel radicals. Schenk et al. [21] stated that under their flame conditions, $C_3H_6$ is formed from the ß-scission of the $iC_4H_9$ radical, which is in turn formed via H-atom addition to the fuel. In the present model and at the conditions studied here, the aforementioned reaction pathway contributes with only 2% to *i*Bu consumption and only 17% to $C_3H_6$ formation. The mole fraction profile of $C_3H_6$ was shown in Fig. 5a, with a maximum that is almost a factor of two lower than for 1Bu. This is quite well represented by the model.

Further differences in the reaction pathways can be observed for $CH_3$ radicals that are a direct result, together with propene, of reaction R1 in 1Bu oxidation. For neat *i*Bu oxidation, $CH_3$ reacts to $CH_4$ via reaction R8, whereas two $CH_3$ radicals predominantly undergo a self-recombination reaction to form $C_2H_6$ in the neat 1Bu oxidation. Ethane, in turn, is then mainly consumed via the reaction sequence $C_2H_6 \rightarrow C_2H_5 \rightarrow C_2H_4$. Ethylene as final product of this reaction sequence reaches a considerably lower mole fraction for the *i*Bu than for the 1Bu case as shown previously in Fig. 5b. This difference is seen both in the measured and in the simulated profiles, underlining the lesser importance of the aforementioned reaction sequence for the neat *i*Bu oxidation.

The $IC_4H_7$ radical is formed preferentially over the fuel radical ($IC_4H_7$-I1) because of its weaker C-H bond [65]. In the *i*Bu oxidation, the formation of $C_4H_6$ is of minor importance compared to the other decomposition pathways and therefore not shown in the ROP analysis in Fig. 9. A significantly lower $C_4H_6$ mole fraction was thus detected for *i*Bu than for 1Bu, as shown in Fig. 5d (please note the different y-axis scales). This is also in accordance with results of Schenk et al. [21]. At temperatures below the $CH_2O$ peak temperature (therefore not shown in the ROP analysis), the dimerization reaction forming 2,5-dimethyl,1-5-hexadiene ($C_8H_{14}$) is the dominant reaction inhibiting the reactivity. The stable species $C_8H_{14}$ was experimentally detected and its mole fraction profile is shown in Fig. 11b.

With increasing temperature, this reaction becomes less important while $IC_4H_7$ decomposes instead with 72% via reaction R10, which is chain-propagating, to $C_3H_4$-A and $CH_3$ radicals.

The formation of $C_3H_4$-A (reaction R10) is the most sensitive reaction in the *i*Bu oxidation at the $CH_2O$ peak temperature as shown in the sensitivity analysis in Fig. 10b. However, reaction R10 is very slow, and only small amounts of $C_3H_4$-A were measured experimentally. Similar as for the 1Bu oxidation, $C_3H_4$-A (Fig. 7a) converts to $C_3H_4$-P (Fig. 7b) by an H-catalyzed isomerization reaction. The measured mole fraction profiles are in accordance with the model predictions, and the temperature-dependent mole fraction profiles reveal that the formation of $C_3H_4$-A and $C_3H_4$-P is favored above 1000 K. Propyne decomposes forming either $C_3H_3$ or $C_2H_2$, while the latter was also detected experimentally (Fig. 7c).

More important than the previously discussed reaction R10 is reaction R11 forming $IC_4H_7O$ and OH radicals, which contributes with 12% to the consumption of the $IC_4H_7$ radicals. Reaction R11 promotes the system's reactivity because $HO_2$ radicals are converted to reactive OH radicals which is in accordance with recent results of Zhou et al. [65], as already discussed in Section 4.1. The $IC_4H_7O$ radical decomposes quickly to methacrolein ($IC_3H_5CHO$) which is further oxidized forming $IC_3H_5CO$. The latter species decomposes to $C_3H_5$-T and finally to CO which significantly promotes the reactivity.

A comparison of the suite of species profiles as well as the ROP and sensitivity analyses has shown considerable differences for the main reaction sequences of both neat fuels which show important reactivity mainly in the temperature region above 900 K. The observed trends have mostly been quite well represented by the present model, and differences in the mole fraction maxima could be understood in terms of the dominant and sensitive reactions. The findings are in general accord with previous studies in the literature of relevance for the present work. On this basis, the interactions of both neat fuels with NO will now be discussed.

#### 4.2.2. 1-Butene and i-Butene oxidation with NO addition

The following analysis will focus on the changes in the oxidation chemistry of the butene isomers introduced by NO addition under the conditions of the present study. Similar as for the neat fuel cases, the discussion will combine information from the reaction flow analyses provided in Figs. 8 and 9, considering also the additional reactions caused by NO addition, with results from mole fraction profiles of relevant hydrocarbon, oxygenated and nitrogen-containing species. The mole fraction profiles for the formerly mentioned species have been already presented in Section 4.1 included in Figs. 1, 2, 5, 7 and 11b together with those for the two neat fuels, and for the latter, selected results are presented in Figs. 11a and 12. Furthermore, a sensitivity analysis for the 1Bu/NO and *i*Bu/NO cases is given in Fig. 13.

*1-Butene oxidation with NO.* Similar to the 1Bu oxidation without NO addition, the first fuel consumption steps in the oxidation of the 1Bu/NO mixture are the radical-initiated H-abstraction reactions R1-R3, and we will discuss their influence sequentially as was done before in Section 4.2.1 for the neat fuel. As evident in Fig. 1a, the fuel consumption in the 1Bu/NO case starts at lower temperatures than for *i*Bu/NO, similar to the difference in onset temperature for the neat fuels.

For neat 1Bu oxidation, the conversion of the fuel is initiated at 886 K, corresponding to about 10% conversion, by its reaction with OH radicals (reaction R2 and R3), where reaction R2 is the dominant reaction pathway. The initial source of the OH radicals in the 1Bu oxidation is the reaction R5 (in this reaction, $HO_2$ radicals are converted to OH radicals). In the presence of NO, however, the formation of OH radicals is initiated via the reactions $O_2+H=O+OH$ and $HO_2CH_2CO=CO+CH_2O+OH$. The well-studied [33,46] interchanging reaction R7 contributes significantly to the OH radical pool both at 50% fuel conversion and at the $CH_2O$ peak temperature according to the ROP analyses. The importance

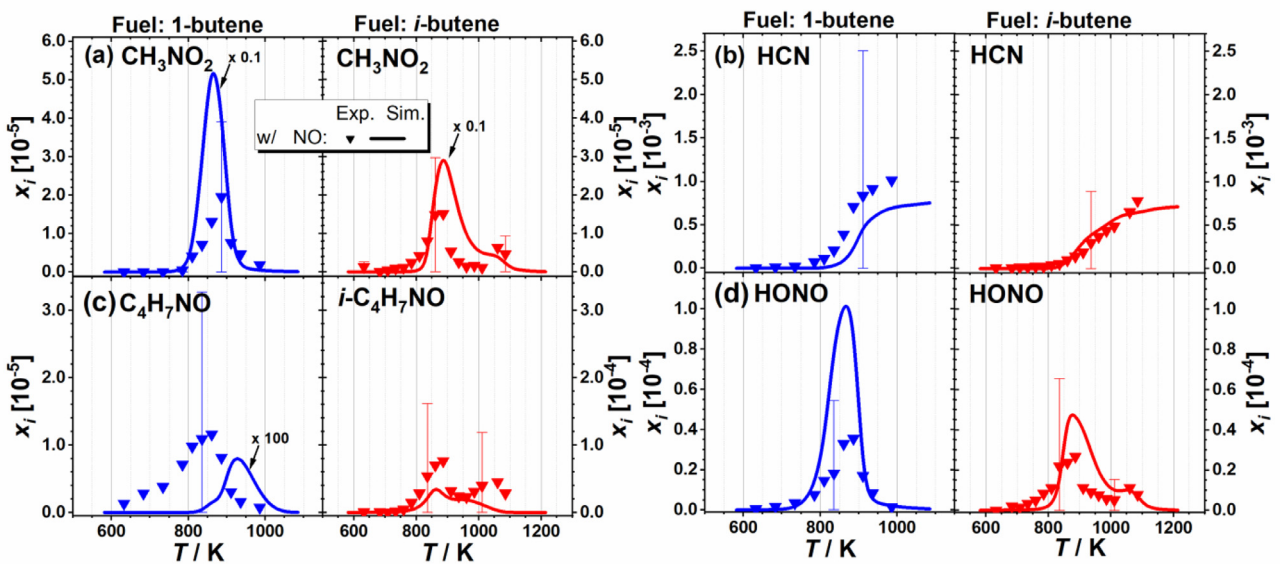


**Fig. 12.** Experimental and simulated mole fractions of (a) $CH_3NO_2$, (b) HCN, (c) $C_4H_7NO$ and (d) HONO in the oxidation of 1Bu (left) and *i*Bu (right) with NO (Exp: square, Sim.: solid line) as a function of temperature. For clarity, experimental uncertainties are given as error bars only at selected temperatures.

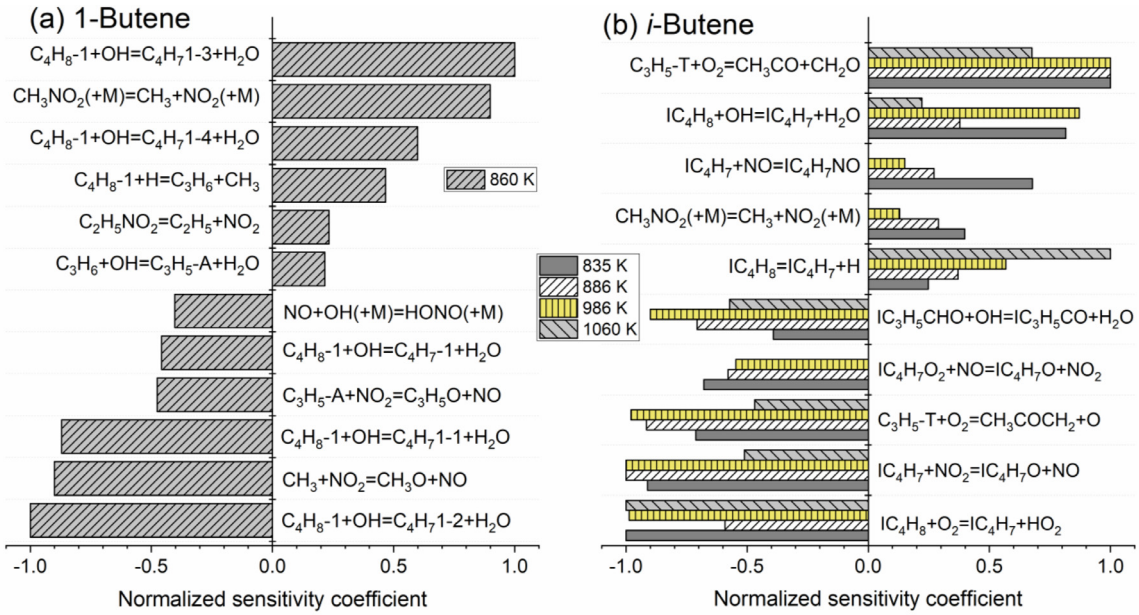


**Fig. 13.** Sensitivity analysis for (a) 1Bu in the 1Bu/NO mixture at 860 K (90% fuel conversion) and for (b) *i*Bu in the *i*Bu/NO mixture at 835 (8%), 886 (54%), 986 (44%), and 1060 K (85%). Reactions represented with a negative normalized sensitivity coefficient enhance fuel consumption, while reactions represented with a positive normalized sensitivity coefficient inhibit the reactivity instead.

of this reaction is underlined by the measurements indicating that NO is rapidly consumed and $NO_2$ is produced, as shown previously in Fig. 1c-d, Section 4.1.

Following the fuel decomposition sequences, reaction R1 leads to propene and $CH_3$ radicals ($C_4H_8$-1+H=$C_3H_6$+$CH_3$), and these products and their further reactions are now inspected for the 1Bu/NO case. The mole fraction profile of $C_3H_6$ as a dominant fuel decomposition product can be compared in Fig. 5a for 1Bu and the 1Bu/NO mixture. NO addition shifts the $C_3H_6$ peak temperature significantly towards lower temperatures. Different from the neat 1Bu case where it is only relevant at temperatures above 900 K, the simulation results confirm that $C_3H_6$ is mainly produced at low temperatures for the 1Bu/NO mixture. $C_3H_6$ is mainly consumed (with 29%) forming $C_3H_5$-A at the $CH_2O$ peak temperature (860 K), which then reacts predominantly (with 69%) further via reaction R16:

$$C_3H_5\text{-A} + NO_2 = C_3H_5O + NO \quad \text{(R16)}$$

$C_3H_5O$ decomposes to acrolein ($C_2H_3CHO$) and H-atom, contributing to the radical pool and making this reaction sequence chain-branching. It can thus contribute to the low-temperature reactivity as was also found for the propene/$O_2$/$NO_x$ mixture [45]. Above the $CH_2O$ peak temperature at 860 K, $C_3H_6$ mainly decomposes at 1035 K to $C_2H_4$ and $CH_3$ with 32% (not shown in the ROP analysis). This pathway is, however, of minor importance compared to the $C_3H_5$-A formation pathway at low temperature.

The predicted profile shape of $C_2H_4$ shown in Fig. 5b differs significantly from the experimental one at temperatures above 800 K, while this species was well predicted in the neat 1Bu case. This difference is also revealed in the ROP analy-

sis in Fig. 8. For neat 1Bu oxidation, $C_2H_4$ is with 86% mainly produced at the $CH_2O$ peak temperature of 1035 K, and only small amounts of $C_2H_4$ are consumed via the reaction sequence $C_2H_4 \rightarrow C_2H_3 \rightarrow CH_2O \rightarrow HCO \rightarrow CO$. In contrast, $C_2H_4$ is produced only with 63% at 1035 K during the oxidation of the 1Bu/NO mixture, which is above the $CH_2O$ peak temperature, resulting in a lower-predicted $C_2H_4$ mole fraction.

Upon NO addition to 1Bu, the $CH_3$ radicals that are predominantly formed via reaction R1 undergo further reactions with $NO_2$ forming reactive $CH_3O$ radicals ($CH_3+NO_2=CH_3O+NO$). As seen from the sensitivity analysis in Fig. 13a, this is one of the most sensitive reactions at the $CH_2O$ peak temperature. Another important reaction is that of $CH_3$ radicals with $O_2$ leading to $CH_3O_2$ radicals; these react further via the interchanging reaction between $CH_3O$ and $CH_3O_2$ radicals enhancing the low-temperature reactivity of HC and NO as has been studied extensively before [33,37,46].

According to the model, the recombination reaction of $CH_3$ and $NO_2$ forming nitromethane ($CH_3NO_2$) is chain-terminating as revealed by the sensitivity analysis in Fig. 13a. This recombination reaction is one of the most important reactions in $CH_3$ radical consumption. Nitromethane was experimentally measured for the 1Bu/NO mixture and its mole fraction profile is shown in Fig. 12a. The shape of the measured mole fraction profile of $CH_3NO_2$ is represented satisfactorily by the model, while its maximum is obviously over-predicted.

Starting from the $C_4H_7$1-3 radicals (produced via reaction R2) in the 1Bu case, it was seen that reaction R4 forming $C_4H_6$ and $HO_2$, is the main consumption pathway at the $CH_2O$ peak temperature. For the 1Bu/NO mixture, however, the $C_4H_7$1-3 radicals mainly react with $NO_2$, forming $C_4H_7$1-O radicals. The reaction of $C_4H_7$1-3 radicals with NO producing $C_4H_6$ is less relevant for the consumption of this fuel radical. The mole fraction profiles of $C_4H_6$ for 1Bu and 1Bu/NO can be compared in Fig. 5d; they are both quite well represented by the model. A decrease of about 50 K is observed in the temperature of the $C_4H_6$ maximum for 1Bu/NO versus neat 1Bu oxidation, where $C_4H_6$ peaks above 900 K. The reaction sequences involving $C_4H_6$ are quite different for the cases with and without NO. According to the ROP analysis, $C_4H_6$ is with 50% mainly produced via $C_4H_7$1-4 and with 29% via reaction R4 in the neat 1Bu oxidation. In contrast, for the 1Bu/NO mixture, $C_4H_6$ is with about 40% mainly formed via the oxygenated species $C_4H_7$1–4$O_2$, which is relevant at lower temperatures. $C_4H_6$ decomposition reactions can produce either $C_3H_4$-A or $C_4H_5$-I. For the 1Bu/NO mixture, the main decomposition pathway of $C_4H_6$ is the formation of $C_4H_5$-I, which, in turn, reacts further via the reaction sequence $C_4H_5\text{-I} \rightarrow C_2H_3CO \rightarrow C_2H_3 \rightarrow CH_2O \rightarrow HCO \rightarrow CO$. Note that it was not possible to detect $C_2H_3$ in the present experiment. Formaldehyde was measured experimentally and was shown in Fig. 2b. The dominant formation pathway of formaldehyde, however, is via the reaction sequence $CH_3 \rightarrow CH_3O \rightarrow CH_2O$. The $CH_3$ radicals are predominantly produced with 42% via reaction R1. The $CH_3$ radicals further react with $NO_2$, forming with 72% $CH_3O$ radicals and NO. The $CH_3O$ radicals finally react with 90% to $CH_2O$.

According to the model, $C_2H_3$ is oxidized by $O_2$ forming $CH_2CHO$, which is of considerable importance for the formation of hydrogen cyanide (HCN) via reaction R18. Another reaction sequence forming HCN is reaction R19 of the $C_2H_3$ radical with NO:

$$CH_2CHO + NO = HCN + HOCHO \quad (R18)$$

$$C_2H_3 + NO = HCN + CH_2O \quad (R19)$$

The mole fraction profile of HCN, which is shown in Fig. 12b, can be captured well by the model. At 1000 K, however, the model under-predicts the mole fractions by about 25 ppm. Obviously, HCN is produced in significant amounts in the 1Bu/NO oxidation. The formation of HCN must be urgently avoided because of its high human toxicity even at low concentrations [68]. For exhaust gas reactions under pre-turbine positioning, temperatures up to 823 K should be considered as technically relevant. Zengel et al. [69] have recently drawn attention on the formation of HCN in lean-burn natural gas engines using different catalytic converters for fast and standard $NH_3$ selective catalytic reduction. In the most unfavored case, up to 30 ppm HCN was produced in a temperature range of 473–523 K. At higher temperatures, up to 17 ppm HCN was measured at 773 K dependent on the catalytic converter. In our study, without catalytic converter, about 71 ppm HCN was detected at 784 K for the 1Bu/NO mixture. This finding is considered as highly relevant for fuel oxidation processes in internal combustion engines where gas-phase reactions might occur in the exhaust aftertreatment.

Mole fraction profiles of further nitrogen-containing species are shown in Fig. 12 and differences with regard to sensitive reactions will be discussed below in comparison with the oxidation of the *i*Bu/NO mixture.

i-*Butene oxidation with NO.* It was already pointed out in Section 4.1 that the main difference introduced by the addition of NO to *i*-butene oxidation under the present conditions is the occurrence of an NTC behavior, which is evident from the fuel consumption and $CH_2O$ profiles shown in Fig. 2b and reasonably well predicted by the kinetics model. A distinct NTC-behavior can also be seen in the $O_2$, $CO_2$ and $H_2O$ profiles presented in Fig. 2, Section 4.1, for which the present model generally represents the experimental results and trends well for all four investigated cases. Hydrocarbon species are mainly relevant at temperatures above 800 K, with no significant shifts to lower temperatures, however, in contrast to the 1Bu/NO case. Most features are reasonably well captured by the model. It will thus be interesting to analyze the reaction sequences that give rise to the observed changes with additional emphasis also on the nitrogenous species.

Concerning the reactivity of the *i*Bu/NO system, the formation of reactive OH radicals is of interest. At the initiation temperature of 969 K, corresponding to about 10% butene conversion in the neat *i*Bu oxidation, the most important source of the OH radical is the reaction $CH_3+HO_2=CH_3O+OH$. As a consequence of the addition of NO, the most important source of OH radicals for the *i*Bu/NO mixture at 835 K is the interchanging reaction R7, leading to an increase of the system's reactivity.

Similar to the neat *i*Bu case, the radical-initiated H-abstraction reaction is the first consumption step also in the *i*Bu/NO oxidation. It forms the resonance-stabilized $IC_4H_7$ radical dominantly via reactions R8 and R9. In addition, this species can be produced also by reaction R20:

$$IC_4H_8 + O_2 = IC_4H_7 + HO_2 \quad (R20)$$

Reaction R20 was found to be the most sensitive reaction below the NTC region and again above 886 K as shown in Fig. 13b. The unreactive $HO_2$ radicals formed are consumed by about 93% through the interchanging reaction $NO+HO_2=NO_2+OH$, producing important OH radicals. The OH radicals are, in turn, mainly consumed via reaction R9, increasing the fuel reactivity. $IC_4H_7$ radicals can be removed via the dimerization reaction R21:

$$IC_4H_7 + IC_4H_7 = H15DE25DM(C_8H_{14}) \quad (R21)$$

This reaction is important below the $CH_2O$ peak temperature; it forms the stable species $C_8H_{14}$, which is chain-terminating and inhibits the reactivity at these temperatures. The mole fraction profile of $C_8H_{14}$ was shown in Fig. 11b. Detectable mole fractions of this species were only found for the cases of *i*Bu with and without NO addition with no significant differences seen in the mole fraction profiles. They are generally represented well by the model,

which predicts slightly lower peak temperatures, however, than observed in the experiment. From the ROP analyses, it is suggested that the formation of $C_8H_{14}$ is more relevant for the neat *i*Bu oxidation than for the *i*Bu/NO mixture.

At the first $CH_2O$ peak temperature, the reaction of the $IC_4H_7$ radical with $HO_2$ radicals, which is relevant in the neat *i*Bu oxidation forming $IC_4H_7O$, is of minor importance for the *i*Bu/NO mixture. Instead, the fuel radical $IC_4H_7$ mainly reacts with $NO_2$ and produces $IC_4H_7O$ radicals via reaction R12 that releases NO. Its contribution to the consumption of the $IC_4H_7$ radicals at the $CH_2O$ peak (886 K) is with 77% significant. With increasing temperature, the contribution of reaction R12 to $IC_4H_7$ consumption decreases considerably, however, because it has a negative temperature dependence, as shown in Fig. S2 in SM1. Reaction R12 was also found to be the second-most sensitive reaction as shown in Fig. 13b. The Arrhenius parameters for reaction R12 were estimated in analogy to those for the similar reaction $C_3H_5$-A+$NO_2$→$C_3H_5O$+NO, which was found to be responsible for the low-temperature reactivity in the 1Bu/NO mixture as well as in the oxidation of the propene/$O_2$/$NO_x$ mixture [45]. However, discrepancies between experiment and simulation that are observed for the fuel consumption (compare Fig. 1a, Section 4.1) indicate that the Arrhenius parameters must probably be inspected more closely. This is, however, beyond the scope of the present study and the reaction should therefore be studied in more detail in the future.

Note that the $IC_4H_7$ and $IC_4H_7O$ radicals could not be detected in the present experiments. However, the stable species $IC_4H_7NO$ and $IC_4H_7NO_2$, which are formed in low amounts (mole fractions of order $10^{-5}$) by the recombination reactions of $IC_4H_7$ with NO and $NO_2$, were detected experimentally and their mole fraction profiles are provided in Figs. 12c and 11a. The NTC behavior was observed for $IC_4H_7NO$. The model predicts the observed trends for $IC_4H_7NO$ and $C_4H_7NO$ in the 1Bu/NO and *i*Bu/NO mixtures quite reasonably (see Fig. 12c). According to the ROP analysis, the formation reactions of $IC_4H_7NO_2$ and $IC_4H_7NO$ are chain-terminating at low temperature. The formation of the $IC_4H_7NO$ radical is also found to be very sensitive at low temperature, as indicated in Fig. 13b. Both reactions compete with a reactive chain sequence initiated by R12. The competition of these reactions lead to the observed NTC region in close similarity to the behavior observed in the previous propene/$NO_x$ investigation [45]. The inhibiting role of $IC_4H_7NO$ is reduced at higher temperatures, where it decomposes to $C_2H_5CHO$ and HCN. This reaction pathway is dominant for the formation of HCN in the *i*Bu/NO mixture at the $CH_2O$ peak temperature. The mole fraction profile of HCN is included in Fig. 12b, and it is very well captured by the model. Again, as for the 1Bu/NO mixture, somewhat smaller but still significant amounts of HCN (23 ppm at 784 K) were produced at temperatures representative of close-coupled engine exhaust aftertreatment systems. Precautions are needed to avoid such emissions because of their toxicity.

As presented in Section 4.2.1 for neat *i*Bu, the $IC_4H_7O$ radicals formed predominantly by reaction R12 decompose quickly to $IC_3H_5CHO$ (methacrolein). For the *i*Bu/NO mixture, the decomposition reaction of methacrolein by H-abstraction to $IC_3H_5CO$ was observed similar to the neat *i*Bu, making this pathway a reactive chain sequence that is believed to be an important contributor to the low-temperature reactivity of the *i*Bu/NO mixture. An additional reaction pathway in the *i*Bu/NO case is the reaction of $IC_3H_5CHO$ with $NO_2$, forming $IC_3H_5CO$ and HONO. Nitrous acid was experimentally detected and its mole fraction profile is shown in Fig. 12d together with that observed in the 1Bu/NO case. Note that details regarding the identification of HONO isomers by photoelectron photoion coincidence spectroscopy have been discussed very recently by Hoener et al. [70]. Such assignment of separate structures was not attempted here, where HONO was detected at a photoionization energy of 11.2 eV.

For the *i*Bu/NO mixture, HONO is mainly formed via the reaction of HNO+$NO_2$=HONO+NO but also from other reaction pathways such as the previously mentioned reaction of $IC_3H_5CHO$ with $NO_2$ with HONO as a product. For both the 1Bu/NO and *i*Bu/NO mixtures, the kinetics model shows respectable agreement between the measured and simulated mole fraction profiles, including the NTC region. $IC_3H_5CO$ decomposes further to $C_3H_5$-T, which can be oxidized to $CH_3CO$ and $CH_2O$:

$$C_3H_5\text{-T} + O_2 = CH_3CO + CH_2O \quad \text{(R23)}$$

Reaction R23 is chain-propagating and contributes to $CH_2O$ formation with 28% at 886 K. According to the sensitivity analysis shown in Fig. 13b, reaction R23 was found to be the most sensitive reaction especially at low temperatures inhibiting the fuel consumption in the NTC region. The formed $CH_3CO$ radical decomposes to a reactive $CH_3$ radical, which, in turn further reacts with $NO_2$ via the reaction $CH_3$+$NO_2$=$CH_3O$+NO. The consumption of $NO_2$ is essential because $NO_2$ is needed for the fuel consumption via reaction R13. Thus, reaction R23 is the major competing reaction to that of the fuel consumption via $IC_4H_7$ radicals (reaction R12) and therefore has a negative sensitivity.

$$C_3H_5\text{-T} + O_2 = CH_3COCH_2 + O \quad \text{(R24)}$$

The $C_3H_5$-T radicals are then oxidized by $O_2$ forming $CH_3COCH_2$ and O radical, which contributes to the radical pool, increasing the fuel reactivity.

The overall enhanced reactivity of 1Bu and *i*Bu upon NO addition can be understood by its contributions to the radical pool. The addition of NO allows the formation of oxygenated species already at low temperature. A main difference between the oxidation of both fuels under the studied conditions is constituted by the reaction pathways of radicals found to be responsible for the low-temperature reactivity, namely, of $C_3H_5O$ radicals for 1Bu and $IC_4H_7O$ radicals for *i*Bu. The NTC region in the *i*Bu case can be explained by the competition of chain-branching and chain-termination reactions of the $IC_4H_7O$ radicals dependent on temperature.

## 5. Conclusions

The oxidation of 1-butene and *i*-butene with and without NO addition were studied systematically at fuel-rich ($\phi$ = 2.0) conditions in flow reactor experiments at atmospheric pressure and temperatures of approximately 600-1200 K using synchrotron-based VUV-PIMS. These studies were performed with a specific interest in the fuel-structure-dependent reaction kinetics as well as in the impact of NO on the respective oxidation rate. Experimental data in form of consistent sets of isomer-resolved species mole fraction profiles were analyzed in detail for two butene isomers with and without NO addition and complemented with simulations using an elementary-step reaction mechanism. The mechanism with the associated kinetic data is based on mechanisms given in literature and extended to obtain all relevant reactions using the experimental data from this work. The model development was further supported by experimental and modeling studies of the oxidation at fuel-lean conditions. The results are provided in the Supplemental Material. The model is thus deemed suitable and in a good starting position to describe interactions between $NO_x$ and hydrocarbons with up to four carbon atoms.

The detailed analysis of the experimental and simulated data reveals that both aspects – the structural differences between the fuels 1-butene and *i*-butene as well as the effects of the NO addition – influence the reactivity due to significant differences in the mixture-specific intermediate species pools and the related changes in respective reaction pathways in the low- to

high-temperature regime. Most obviously, a low-temperature reactivity leading to an NTC region below 1000 K was induced in the *i*-butene/NO mixture, while no NTC behavior was observed for the other mixtures. It was found that the observed NTC region in the *i*-butene/NO mixture can be traced back to the formation of $IC_4H_7O$ radicals that are chain-branching and initiate the low-temperature reactivity. The rate constant of the most important reaction $IC_4H_7+NO_2=IC_4H_7O+NO$ shows a negative temperature coefficient in the *i*-butene/NO mixture, which explains the reduced reactivity with temperature increase. The aforementioned reaction, however, competes with the recombination reactions leading to $IC_4H_7NO_2$ and $IC_4H_7NO$ formation, thus decreasing the reactivity at low temperatures, instead. The inhibiting reactivity is reduced with temperature increase.

The overall enhanced reactivity upon NO addition can be traced back to its contribution on the radical pool for both fuels. These include, for example, the well-known interchanging reactions such as $NO+HO_2=NO_2+OH$ producing important and reactive OH radicals and $CH_3+NO_2=CH_3O+NO$. It was shown that significant amounts of nitrogenated species, including HCN were produced at moderate temperatures and atmospheric pressure relevant to exhaust gas conditions. It is crucial that the formation of toxic HCN is avoided and therefore the occurrence of gas-phase reactions leading to HCN should be considered carefully in technical combustion processes.

Even though the present model reasonably captures the mole fraction profiles for most of the species, prospective improvements and extensions of the model might be considered. The experimental data from the present study are expected to be valuable for the development of such future combustion models.

## Author information

SG, LR, WY, JZ and XC performed the experiments; SG, LR, WY and SS evaluated the data; WY developed the model; SG and WY performed the modeling; SG, LR, WY, SS, and LM performed the kinetics analysis; SG, LR, KKH and OD wrote the paper, KKH, FQ and OD participated in experiment planning, interpretation and discussions and supervised the work.

## Declaration of Competing Interest

The authors declare that they have no known competing financial interests or personal relationships that could have appeared to influence the work reported in this paper.

## Acknowledgments

This research was supported by a NSFC-DFG joint Sino-German research project. Fei Qi acknowledges support from the National Natural Science Foundation of China (51761135111), Katharina Kohse-Höinghaus and Olaf Deutschmann are grateful for support from Deutsche Forschungsgemeinschaft, project number 391765816 (KO 1363/34-1 and DE 659/12-1).

## Supplementary material

Supplementary material associated with this article can be found, in the online version, at doi:10.1016/j.combustflame.2021.111557.

## References

[1] B. Wolk, I. Ekoto, W.F. Northrop, K. Moshammer, N. Hansen, Detailed speciation and reactivity characterization of fuel-specific in-cylinder reforming products and the associated impact on engine performance, Fuel 185 (2016) 348–361.
[2] W.S. Epling, L.E. Campbell, A. Yezerets, N.W. Currier, J.E. Parks, Overview of the fundamental reactions and degradation mechanisms of $NO_x$ storage/reduction catalysts, Catal. Rev. – Sci. Eng. 46 (2004) 163–245.
[3] M.P. Harold, NOx storage and reduction in lean burn vehicle emission control: a catalytic engineer's playground, Curr. Opin. Chem. Eng. 1 (2012) 303–311.
[4] J. Koop, O. Deutschmann, Detailed surface reaction mechanism for Pt-catalyzed abatement of automotive exhaust gases, Appl. Catal. B Environ. 91 (2009) 47–58.
[5] A.M. Gänzler, M. Casapu, F. Maurer, H. Störmer, D. Gerthsen, G. Ferré, P. Vernoux, B. Bornmann, R. Frahm, V. Murzin, M. Nachtegaal, M. Votsmeier, J.D. Grunwaldt, Tuning the Pt/$CeO_2$ interface by in situ variation of the Pt particle size, ACS Catal. 8 (2018) 4800–4811.
[6] A. Gremminger, P. Lott, M. Merts, M. Casapu, J.D. Grunwaldt, O. Deutschmann, Sulfur poisoning and regeneration of bimetallic Pd-Pt methane oxidation catalysts, Appl. Catal. B Environ. 218 (2017) 833–843.
[7] T. Maunula, K. Kallinen, N. Kinnunen, M. Keenan, T. Wolff, Methane abatement and catalyst durability in heterogeneous lean-rich and dual-fuel conditions, Top. Catal. 62 (2019) 315–323.
[8] P. Lott, O. Deutschmann, Lean-burn natural gas engines: challenges and concepts for an efficient exhaust gas aftertreatment system, Emiss. Control Sci. Technol. 7 (2021) 1–6.
[9] K.A. Karinshak, P. Lott, M.P. Harold, O. Deutschmann, In situ activation of bimetallic Pd−Pt methane oxidation catalysts, ChemCatChem 12 (2020) 3712–3720.
[10] J. Smith, J. Phillips, U.V. Park, V. Pennsyl, A. Graham, R. Steele, A. Redondo, J. Coons, Homogeneous Chemistry in Lean-Burn Exhaust Mixtures, 5639 (1997) 9157–9162.
[11] B. Torkashvand, P. Lott, D. Zengel, L. Maier, M. Hettel, J.D. Grunwaldt, O. Deutschmann, Homogeneous oxidation of light alkanes in the exhaust of turbocharged lean-burn gas engines, Chem. Eng. J. (2019) 377.
[12] T. Günter, J. Pesek, K. Schäfer, A.B. Abai, M. Casapu, O. Deutschmann, J. Grunwaldt, Cu-SSZ-13 as pre-turbine NOx-removal-catalyst : impact of pressure and catalyst poisons, Appl. Catal. B Environ. 198 (2016) 548–557.
[13] S. Schmitt, S. Schwarz, L. Ruwe, J. Horstmann, F. Sabath, L. Maier, O. Deutschmann, K. Kohse-Höinghaus, Homogeneous conversion of $NO_x$ and $NH_3$ with $CH_4$, CO, and $C_2H_4$ at the diluted conditions of exhaust-gases of lean operated natural gas engines, Int. J. Chem. Kinet. 53 (2021) 213–229.
[14] M. Tayyeb Javed, N. Irfan, B.M. Gibbs, Control of combustion-generated nitrogen oxides by selective non-catalytic reduction, J. Environ. Manag. 83 (2007) 251–289.
[15] S. Gersen, A.V. Mokhov, J.H. Darmeveil, H.B. Levinsky, P. Glarborg, Ignition-promoting effect of $NO_2$ on methane, ethane and methane/ethane mixtures in a rapid compression machine, Proc. Combust. Inst. 33 (2011) 433–440.
[16] Y. Zhang, J. Cai, L. Zhao, J. Yang, H. Jin, Z. Cheng, Y. Li, L. Zhang, F. Qi, An experimental and kinetic modeling study of three butene isomers pyrolysis at low pressure, Combust. Flame 159 (2012) 905–917.
[17] A. Chakir, M. Cathonnet, J.C. Boettner, F. Gaillard, Kinetic study of 1-butene oxidation in a jet-stirred flow reactor, Symp. Combust. 22 (1989) 873–881.
[18] B. Heyberger, N. Belmekki, V. Conraud, P.-.A. Glaude, R. Fournet, F. Battin-Leclerc, Oxidation of small alkenes at high temperature, Int. J. Chem. Kinet. 34 (2002) 666–677.
[19] S.G. Davis, C.K. Law, Determination of and Fuel Structure effects on laminar flame speeds of C1 to C8 hydrocarbons, Combust. Sci. Technol. 140 (1998) 427–449.
[20] P. Zhao, W. Yuan, H. Sun, Y. Li, A.P. Kelley, X. Zheng, C.K. Law, Laminar flame speeds, counterflow ignition, and kinetic modeling of the butene isomers, Proc. Combust. Inst. 35 (2015) 309–316.
[21] M. Schenk, L. Leon, K. Moshammer, P. Oßwald, T. Zeuch, L. Seidel, F. Mauss, K. Kohse-Höinghaus, Detailed mass spectrometric and modeling study of isomeric butene flames, Combust. Flame 160 (2013) 487–503.
[22] Y. Fenard, P. Dagaut, G. Dayma, F. Halter, F. Foucher, Experimental and kinetic modeling study of trans-2-butene oxidation in a jet-stirred reactor and a combustion bomb, Proc. Combust. Inst. 35 (2015) 317–324.
[23] K. Brezinsky, F.L. Dryer, A flow reactor study of the oxidation of iso-butylene and an lso-butylenein-octane mixture, Combust. Sci. Technol. 45 (1986) 225–232.
[24] J.N. Bradley, M.A. Frend, Single-pulse shock tube studies of hydrocarbon pyrolysis. II. The pyrolysis of ethane, J. Phys. Chem. 75 (1971) 1492–1501.
[25] W. Tsang, J.A. Walker, Mechanism and rate constants for the reactions of hydrogen atoms with isobutene at high temperatures, Symp. Combust. 22 (1989) 1015–1022.
[26] S. Santhanam, J.H. Kiefer, R.S. Tranter, N.K. Srinivasan, A shock tube, laser-schlieren study of the pyrolysis of isobutene: relaxation, incubation, and dissociation rates, Int. J. Chem. Kinet. 35 (2003) 381–390.
[27] K. Yasunaga, Y. Kuraguchi, R. Ikeuchi, H. Masaoka, O. Takahashi, T. Koike, Y. Hidaka, Shock tube and modeling study of isobutene pyrolysis and oxidation, Proc. Combust. Inst. 32 I (2009) 453–460.
[28] P. Dagaut, M. Cathonnet, Isobutene oxidation and ignition: experimental and detailed kinetic modeling study, Combust. Sci. Technol. 137 (1998) 237–275.
[29] V. Dias, J. Vandooren, Experimental and modeling study of a lean premixed iso-butene/hydrogen/oxygen/argon flame, Fuel 89 (2010) 2633–2639.
[30] Y.L. Chan, F.J. Barnes, J.H. Bromly, A.A. Konnov, D.K. Zhang, The differentiated effect of NO and $NO_2$ in promoting methane oxidation, Proc. Combust. Inst. 33 (2011) 441–447.
[31] P. Glarborg, M.U. Alzueta, K. Dam-Johansen, J.A. Miller, Kinetic modeling of hydrocarbon/nitric oxide interactions in a flow reactor, Combust. Flame 115 (1998) 1–27.
[32] C.L. Rasmussen, A.E. Rasmussen, P. Glarborg, Sensitizing effects of $NO_x$ on $CH_4$ oxidation at high pressure, Combust. Flame 154 (2008) 529–545.

[33] T. Faravelli, A. Frassoldati, E. Ranzi, Kinetic modeling of the interactions between NO and hydrocarbons in the oxidation of hydrocarbons at low temperatures, Combust. Flame 132 (2003) 188–207.
[34] A.B. Bendtsen, P. Glarborg, K. Dam-Johansen, Low temperature oxidation of methane: the influence of nitrogen oxides, Combust. Sci. Technol. 151 (2000) 31–71.
[35] Y. Song, L. Marrodán, N. Vin, O. Herbinet, E. Assaf, C. Fittschen, A. Stagni, T. Faravelli, M.U. Alzueta, F. Battin-Leclerc, The sensitizing effects of $NO_2$ and NO on methane low temperature oxidation in a jet stirred reactor, Proc. Combust. Inst. 37 (2019) 667–675.
[36] A.A. Konnov, J. Ning Zhu, J.H. Bromly, D.K. Zhang, The effect of NO and $NO_2$ on the partial oxidation of methane: experiments and modeling, Proc. Combust. Inst. 30 (2005) 1093–1100.
[37] J.H. Bromly, F.J. Barnes, S. Muris, X. You, B.S. Haynes, Kinetic and thermodynamic sensitivity analysis of the NO-sensitised oxidation of methane, Combust. Sci. Technol. 115 (1996) 259–296.
[38] B. Torkashvand, A. Gremminger, S. Valchera, M. Casapu, J.D. Grunwaldt, O. Deutschmann, The Impact of Pre-Turbine Catalyst Placement on Methane Oxidation in Lean-Burn Gas Engines: An Experimental and Numerical Study, 2017 SAE Tech. Pap. 2017-01–10.
[39] P. Dagaut, A. Nicolle, Experimental study and detailed kinetic modeling of the effect of exhaust gas on fuel combustion: mutual sensitization of the oxidation of nitric oxide and methane over extended temperature and pressure ranges, Combust. Flame 140 (2005) 161–171.
[40] J.C. Corchado, J. Espinosa-Garcıá, Analytical potential energy surface for the $NH_3+H \leftrightarrow NH_2+H_2$ reaction: application of variational transition-state theory and analysis of the equilibrium constants and kinetic isotope effects using curvilinear and rectilinear coordinates, J. Chem. Phys. 106 (1997) 4013–4021.
[41] P. Dagaut, G. Dayma, Mutual sensitization of the oxidation of nitric oxide and a natural gas blend in a JSR at elevated pressure: experimental and detailed kinetic modeling study, J. Phys. Chem. A 110 (2006) 6608–6616.
[42] F. Deng, Y. Zhang, W. Sun, W. Huang, Q. Zhao, X. Qin, F. Yang, Z. Huang, Towards a kinetic understanding of the $NO_x$ sensitization effect on unsaturation hydrocarbons: a case study of ethylene/nitrogen dioxide mixtures, Proc. Combust. Inst. 37 (2019) 719–726.
[43] P. Gokulakrishnan, C.C. Fuller, M.S. Klassen, Experimental and modeling study of C1-C3 hydrocarbon ignition in the presence of nitric oxide, J. Eng. Gas Turb. Power 140 (2018).
[44] J. Giménez-López, M.U. Alzueta, C.T. Rasmussen, P. Marshall, P. Glarborg, High pressure oxidation of $C_2H_4$/NO mixtures, Proc. Combust. Inst. 33 (2011) 449–457.
[45] W. Yuan, L. Ruwe, S. Schwarz, C. Cao, J. Yang, O. Deutschmann, K. Kohse-Höinghaus, F. Qi, Insights into the interaction kinetics between propene and NOx at moderate temperatures with experimental and modeling methods, Proc. Combust. Inst. 38 (2021) 795–803.
[46] P.A. Glaude, N. Marinov, Y. Koshiishi, N. Matsunaga, M. Hori, Kinetic modeling of the mutual oxidation of NO and larger alkanes at low temperature, Energy Fuels 19 (2005) 1839–1849.
[47] D. Liu, B.R. Giri, M. Szőri, B. Viskolcz, E. Essbar, A. Farooq, On the redox reactions between allyl radicals and NOx, Proc. Combust. Inst. 38 (2021) 967–976.
[48] S.K. Prabhu, R.K. Bhat, D.L. Miller, N.P. Cernansky, 1-Pentene oxidation and its interaction with nitric oxide in the low and negative temperature coefficient regions, Combust. Flame 104 (1996) 377–390.
[49] Y. Li, C.W. Zhou, H.J. Curran, An extensive experimental and modeling study of 1-butene oxidation, Combust. Flame 181 (2017) 198–213.
[50] J. Cai, L. Zhang, F. Zhang, Z. Wang, Z. Cheng, W. Yuan, F. Qi, Experimental and kinetic modeling study of n-butanol pyrolysis and combustion, Energy Fuels 26 (2012) 5550–5568.
[51] F. Qi, Combustion chemistry probed by synchrotron VUV photoionization mass spectrometry, Proc. Combust. Inst. 34 (2013) 33–63.
[52] Y. Zhang, C. Cao, Y. Li, W. Yuan, X. Yang, J. Yang, F. Qi, T.P. Huang, Y.Y. Lee, Pyrolysis of n-butylbenzene at various pressures: influence of long side-chain structure on alkylbenzene pyrolysis, Energy and Fuels 31 (2017) 14270–14279.
[53] Z. Zhou, X. Du, J. Yang, Y. Wang, C. Li, S. Wei, L. Du, Y. Li, F. Qi, Q. Wang, The vacuum ultraviolet beamline/endstations at NSRL dedicated to combustion research, J. Synchrotron Radiat. 23 (2016) 1035–1045.
[54] S.S. C.R.Narayanan, R.G. A.K.Datye, A. Biaglow, The effect of alumina structure on surface sites for alcohol dehydration, J. Catal. 138 (1992) 659–674.
[55] C.W. Zhou, Y. Li, U. Burke, C. Banyon, K.P. Somers, S. Ding, S. Khan, J.W. Hargis, T. Sikes, O. Mathieu, E.L. Petersen, M. AlAbbad, A. Farooq, Y. Pan, Y. Zhang, Z. Huang, J. Lopez, Z. Loparo, S.S. Vasu, H.J. Curran, An experimental and chemical kinetic modeling study of 1,3-butadiene combustion: ignition delay time and laminar flame speed measurements, Combust. Flame 197 (2018) 423–438.
[56] P. Glarborg, J.A. Miller, B. Ruscic, S.J. Klippenstein, Modeling nitrogen chemistry in combustion, Prog. Energy Combust. Sci. 67 (2018) 31–68.
[57] J. Chai, C.F. Goldsmith, Rate coefficients for fuel + $NO_2$: predictive kinetics for HONO and $HNO_2$ formation, Proc. Combust. Inst. 36 (2017) 617–626.
[58] M.P. Rissanen, D. Amedro, L. Krasnoperov, P. Marshall, R.S. Timonen, Gas phase kinetics and equilibrium of allyl radical reactions with NO and NO2, J. Phys. Chem. A. 117 (2013) 793–805.
[59] M. Hori, N. Matsunaga, N. Marinov, W. Pitz, C. Westbrook, An experimental and kinetic calculation of the promotion effect of hydrocarbons on the NO-$NO_2$ conversion in a flow reactor, Symp. Combust. 27 (1998) 389–396.
[60] M.J. Frisch, G.W. Trucks, H.B. Schlegel, G.E. Scuseria, M.A. Robb, J.R. Cheeseman, G. Scalmani, V. Barone, B. Mennucci, G.A. Petersson, H. Nakatsuji, M. Caricato, X. Li, H.P. Hratchian, A.F. Izmaylov, J. Bloino, G. Zheng, J.L. Sonnenberg, M. Hada, M. Ehara, K. Toyota, R. Fukuda, J. Hasegawa, M. Ishida, T. Nakajima, Y. Honda, O. Kitao, H. Nakai, T. Vreven, J.A.M. Jr., J.E. Peralta, F. Ogliaro, M. Bearpark, J.J. Heyd, E. Brothers, K.N. Kudin, V.N. Staroverov, R. Kobayashi, J. Normand, K. Raghavachari, A. Rendell, J.C. Burant, S.S. Iyengar, J. Tomasi, M. Cossi, N. Rega, J.M. Millam, M. Klene, J.E. Knox, J.B. Cross, V. Bakken, C. Adamo, J. Jaramillo, R. Gomperts, R.E. Stratmann, O. Yazyev, A.J. Austin, R. Cammi, C. Pomelli, J.W. Ochterski, R.L. Martin, K. Morokuma, V.G. Zakrzewski, G.A. Voth, P. Salvador, J.J. Dannenberg, S. Dapprich, A.D. Daniels, O. Ortiz, J. Cioslowski, D.J. Fox, Gaussian 09, (Gaussian, Inc., Wallingford CT, 2009).
[61] E.R. Ritter, J.W. Bozzelli, THERM: thermodynamic property estimation for gas phase radicals and molecules, Int. J. Chem. Kinet. 23 (1991) 767–778.
[62] S.M. Burke, J.M. Simmie, H.J. Curran, Critical evaluation of thermochemical properties of C1-C4species: updated group-contributions to estimate thermochemical properties, J. Phys. Chem. Ref. Data 44 (2015) 013101.
[63] *Ansys*® CHEMKIN-Pro, Release 2020 R2.
[64] Y.-R. Luo, Comprehensive Handbook of Chemical Bond Energies, CRC Press, Boca Raton, FL, 2007.
[65] C.W. Zhou, Y. Li, E. O'Connor, K.P. Somers, S. Thion, C. Keesee, O. Mathieu, E.L. Petersen, T.A. DeVerter, M.A. Oehlschlaeger, G. Kukkadapu, C.J. Sung, M. Alrefae, F. Khaled, A. Farooq, P. Dirrenberger, P.A. Glaude, F. Battin-Leclerc, J. Santner, Y. Ju, T. Held, F.M. Haas, F.L. Dryer, H.J. Curran, A comprehensive experimental and modeling study of isobutene oxidation, Combust. Flame 167 (2016) 353–379.
[66] F. Khaled, B.R. Giri, A. Farooq, A high-temperature shock tube kinetic study for the branching ratios of isobutene + OH reaction, Proc. Combust. Inst. 36 (2017) 265–272.
[67] X.L. Zheng, H.Y. Sun, C.K. Law, Thermochemical and kinetic analyses on oxidation of isobutenyl radical and 2-hydroperoxymethyl-2-propenyl radical, J. Phys. Chem. A 109 (2005) 9044–9053.
[68] E. Jaszczak, Ż. Polkowska, S. Narkowicz, J. Namieśnik, Cyanides in the environment—analysis—problems and challenges, Environ. Sci. Pollut. Res. 24 (2017) 15929–15948.
[69] D. Zengel, P. Koch, B. Torkashvand, J.D. Grunwaldt, M. Casapu, O. Deutschmann, Emission of toxic HCN during NOx removal by ammonia SCR in the exhaust of lean-burn natural gas engines, Angew. Chem. – Int. Ed. 59 (2020) 14423–14428.
[70] M. Hoener, A. Bodi, P. Hemberger, T. Endres, T. Kasper, Threshold photoionization shows no sign of nitryl hydride in methane oxidation with nitric oxide, Phys. Chem. Chem. Phys. 23 (2021) 1265–1272.